REPUBLIC OF TÜRKİYE
AYDIN ADNAN MENDERES UNIVERSITY
GRADUATE SCHOOL OF NATURAL AND APPLIED SCIENCES
MASTER’S PROGRAMME IN MECHANICAL ENGINEERING
2023-YL-059

EFFECT OF MATERIAL CHANGE AT PLATE HEAT EXCHANGER DESIGN TO SYSTEM PERFORMANCE

KADİR CEBECİ
MASTER’S THESIS

SUPERVISOR

Asst. Prof. Dr. Sinan GÜÇLÜER

AYDIN–2023

APPROVAL AND ACCEPTANCE

The thesis titled "EFFECT OF MATERIAL CHANGE AT PLATE HEAT EXCHANGER DESIGN TO SYSTEM PERFORMANCE" was prepared by the Kadir CEBECİ, a student of the Department of Mechanical Engineering at T.C. Aydın Adnan Menderes University, Graduate School of Natural and Applied Science was accepted as a Master's Thesis by the jury below.

Date of Thesis Defence: 18/07/2023

	Title, Name Surname	**Institution**	**Signature**
Member: (T.D.)	Asst. Prof. Dr. Sinan GÜÇLÜER	Aydın Adnan Menderes University	
Member:	Assoc. Prof. Dr. Adem ÖZÇELİK	Aydın Adnan Menderes University	
Member:	Asst. Prof. Dr. Fikret SÖNMEZ	Manisa Celal Bayar University	

APPROVAL:

This thesis was approved by the jury above under the relevant articles of the Aydın Adnan Menderes University Graduate Education and Examination Regulations and was approved on the .... by from the Board of Directors of the Graduate School of Science in the .... numbered decision.

Prof. Dr. Mustafa SÜRMEN

Institute Director

ACKNOWLEDGEMENTS

I would like to express my sincere gratitude to my advisor Asst. Prof. Dr Sinan Güçlüer, for their invaluable guidance and support throughout my master's program. Their expertise and encouragement helped me to complete this research and write this thesis.

I would like to express my appreciation to Atalay Tunç and Yiğit Gürler for giving me the chance to carry out my study at BOSCH Home Comfort Group and for all the resources and assistance that they made available to me during that time.

I would like to acknowledge my colleagues at BOSCH Home Comfort Group for their support and assistance throughout my research.

I would like to acknowledge Berkay Türkcan Imrağ and Çınar Guris for their assistance with finite element analysis and conducted experiments, respectively.

I would want to thank my parents, and my brother for all the love and support they have given me.

Finally, I would like to express my utmost gratitude to my wife, Feyza Nur Cebeci, for the unwavering support and consistent encouragement that she has given me during the process of conducting research and producing my thesis.

Kadir CEBECİ

TABLE OF CONTENTS

LIST OF SYMBOLS AND ABBREVIATIONS

C-PHE : Compact Plate Heat Exchanger
CH : Central Heating
DCW : Domestic Cold Water
DHW : Domestic Hot Water
mm : Millimeter
PHE : Plate Heat Exchanger
FEA : Finite Element Analysis
FEM : Finite Element Method
PPD : Plastic Protecting Device
kW : Kilowatt
FE : Finite Element
AI : Artificial Intelligence
BPHE : Brazed Plate Heat Exchanger
GPa : Gigapascal
AISI : American Iron and Steel Institute
1D : One-Dimensional
2D : Two-Dimensional
3D : Three-Dimensional
FEM : Finite Element Method
CAD : Computer Aided Design
MPa : Megapascal
Nom : Nominal
Min : Minimum
Max : Maximum
kg : Kilogram

LIST OF FIGURES

LIST OF TABLES

ÖZET

PLAKALI EŞANJÖR TASARIMINDA MALZEME DEĞİŞİKLİĞİNİN SİSTEM PERFORMANSINA ETKİSİ

Cebeci K. Aydın Adnan Menderes Üniversitesi, Fen Bilimleri Enstitüsü, Makine Mühendisliği Programı, Yüksek Lisans Tezi, Aydın, 2023.

Amaç: Bu araştırma, plakalı eşanjörlerin üst plakasında alternatif malzeme kullanımı ve bu kullanımın bileşen performansına olan etkisinin incelenmesi amacı ile yapılmıştır.

Materyal ve Yöntem: Araştırma, AISI 316L ve AISI 304L paslanmaz çelik malzemelerinin kullanıldığı plakalı eşanjörler ile gerçekleştirilmiştir. Performans parametresi olarak farklı malzeme içeriğine sahip ürünlerin termal performans değerleri ve patlama dayanım kriterleri ele alınmıştır. Termal performans plakalı eşanjör fonksiyonel test standında gerçekleşmiştir. Maximator basınçlandırma kiti ve plakalı eşanjör sabitleme aparatı ile patlama dayanım testleri uygulanmıştır. ANSYS FEA analizi ile sonuçları doğrulayan bir simülasyon metodu geliştirilmiştir. Test sonucunda elde edilen dayanım kriterleri, geliştirilen numerik metotla analiz edilmiş ve ilgili bulgular arasındaki korelasyon değerlendirilmiştir.

Bulgular: Araştırmada farklı kalınlıkta ve tipte paslanmaz çelik malzemeler kullanılarak üretilmiş olan numunelerin, termal verimlilikleri ve plastik deformasyon basınçları tanımlanmıştır. AISI 316L malzeme ile üretilen üst plakadaki deformasyon başlangıcı 24 bar, AISI 304L malzeme ile üretilen üst plakadaki gözle görülen deformasyon başlangıcı 18 bar olarak belirlenmiştir.

Sonuç: Kalınlığı azaltılmış 0,5 mm AISI 316L ve AISI 304L üst plaka ile üretilmiş olan plakalı ısı eşanjörlerinin mekanik dayanım performanslarının seri üretime uygun olduğu ve benzer şekilde her iki malzemenin termal performans testinde olumlu sonuçlar verdiği sonucuna ulaşılmıştır.

Anahtar Kelimeler: Kompakt Plakalı Isı Eşanjörü, Mekanik Özellikler, Patlatma Testi.

ABSTRACT

EFFECT OF MATERIAL CHANGE AT PLATE HEAT EXCHANGER DESIGN TO SYSTEM PERFORMANCE

Cebeci K. Aydın Adnan Menderes University, Graduate School of Natural and Applied Sciences, Mechanical Engineering Program, Master Thesis, Aydın, 2023

Objective: The objective of this research was to examine the use of alternative materials on the top plate of plate heat exchangers and their influence on the operational effectiveness of the component.

Material and Methods: The research was carried out with plate heat exchangers using AISI 316L and AISI 304L stainless steel materials. Thermal performance values and burst resistance criteria of products with different material content are considered as performance parameters. The thermal performance was realized in the plate heat exchanger functional test stand. Pressure resistance tests were carried out with Maximator pressurization kit and plate heat exchanger fixing apparatus. A simulation method has been developed that validates the results with ANSYS FEA analysis. The obtained strength criteria were subjected to analysis using a numerical method that was developed for this purpose. The correlation between the relevant findings was assessed.

Results: In the study, thermal efficiencies and plastic deformation pressures of samples manufactured from various varieties of steel were determined. The beginning of deformation in the AISI 316L-made top plate was determined to be 24 bar, while the deformation in the AISI 304L-made top plate was determined to be 18 bar.

Conclusion: The study determined that the plate heat exchangers manufactured using 0.5 mm AISI 316L and AISI 304L top plates with reduced thickness exhibit mechanical strength performance that is conducive to large-scale production. Additionally, both materials demonstrated favorable outcomes in the thermal performance evaluation.

Key Words: Compact Plate Heat Exchanger, Mechanical Properties, Burst Test Deformation.

1. INTRODUCTION

Plate heat exchangers are utilized as a component of residential comfort systems, offering convenient access to heated water. The increase in market demand for these solutions has resulted in challenges related to the availability of the necessary materials. The significance of exploring alternative materials in various industries cannot be overstated. It provides a strategic advantage for maintaining production through shiftability. Daily, there is a rise in the prices of materials. To counter this issue, it is imperative to implement cost-efficient, intelligent solutions. The primary goals of central heating system invention were to reduce used volume and increase output from the start. Compact plate heat exchangers have been introduced to the market with the aim of fulfilling this purpose, following years of advancements. They were and are crucial parts of natural gas combi boilers. This system efficiently delivers heated water to customers within a short period of time. Various companies are currently conducting studies on alternative materials for this component, taking into consideration factors such as availability and cost. Compact plate heat exchangers consist of internal plates for channel routing, copper foils for brazing, and top and cover plates for enclosure. The necessary thermal output of a plate heat exchanger is not solely dependent on the primary heat exchanger but also on the heat transfer rate between the internal plates, which is influenced by the temperature differential of the CH line. Hence, it is imperative to utilize materials that exhibit commendable brazing and formability characteristics, particularly for internal plates. Various types of materials are available for brazing purposes. Metals such as copper and nickel are examples of elements commonly used in various applications. The criteria for selecting brazing materials are primarily associated with the operational circumstances, the size of the plate heat exchanger, and the chosen brazing technique. To ensure the durability of covers during transportation, it is necessary to utilize materials that possess both strong damage resistance and favorable formability properties. Furthermore, optimal formability properties are also essential for the fabrication of patterns in materials. To achieve a welded connection between end plates and inner plates in PHE, it is imperative to have good brazing properties. By conducting a study on alternative materials for plate heat exchangers, it is possible to identify cost-effective options that can be incorporated into the inventory. Various tests with distinct methodologies are available for conducting functionality and system performance analyses of the PHE.

Functional tests are performed on finished products to measure the temperature delta and determine the output value and efficiency of the component. Water hammer tests utilizing dynamic loads are employed to replicate the domestic water usage cycle executed by consumers. Lifetime tests are utilized to determine the lifespan of the system. Burst tests that involve static loads resulting from domestic pressure and a designated application time are currently employed for:

- Identification of the maximum burst pressure,
- Design margin confirmation of the production part,
- Factor of safety evaluation,
- Failure mode determination (the way in which a part fails),
- Finding the ‘weakest link’ in a production or assembly.

The assessment of the burst performance of a product is contingent upon the successful execution of production operations such as stamping and brazing. It is imperative to ensure that these operations are carried out with precision, as any misalignment can result in a weakened link in the brazed points. This phenomenon has been thoroughly examined and analyzed in Yiğit Gürler's master's thesis study. The presence of significant domestic pressure poses a risk to the integrity of the indicated links, potentially resulting in the occurrence of internal leakage. Furthermore, in the process of selecting materials for this study, the master's thesis study conducted by Yiğit Hayta, containing valuable insights on metal forming and mechanical property analysis, was utilized as a point of reference. The execution of burst tests necessitates the availability of a fully developed product, which can be deemed disadvantageous in relation to the expenses and exertions associated with product development. The objective of this investigation is to conduct a finite element analysis (FEA) that is appropriate for simulating the burst effect observed in the experiment. This novel study eliminates the necessity for material disposal in relation to said test. It will be feasible to examine various cover plates featuring distinct surface patterns. The outputs will provide the engineer with pertinent information regarding the shape, pattern, grain size, or mechanical properties that are necessary for the intended use case.

1.1. Central Heating System History

During the 13th century, the ancient Greeks formulated a concept that may be considered as a form of central heating. Temples were equipped with a heating system that utilized the heat generated by fire and circulated it through flues. Furthermore, the ancient Romans employed a comparable method of heating entire rooms through the use of furnaces and the circulation of heated air throughout walls and beneath floors. The hypocaust is a subterranean space situated beneath stone flooring that is utilized to facilitate the circulation of heated air. Recent findings suggest that Asia was the first known originator of these systems, predating the Romans by several millennia. Commencing with the excavated floor flues of antiquated Korea and progressing towards the hypocausts of the Greek and Roman civilizations, as well as comparable systems employed in the Middle Eastern region.1 During the year 1300 B.C, King Arzawa implemented a system within his palace located in Beycesultan, Turkey.

In the 1700s, stoves began to be utilized as a source of heating after years of advancements and enhancements. The main disadvantage associated with stoves was their limited capacity to provide heat to a single room exclusively. Following the discovery of coal as a viable heat source and the beginning of the Industrial Revolution, heating technology advanced significantly, leading to the invention of radiators in the 1800s. One such heating device that emerged during this period was the 'Hot Box.'

The first functional central boiler system was constructed by the Scottish innovator James Watt within his residence. The inventor's creation entailed the utilization of high-pressure steam, which was subsequently dispersed via a network of pipes. Watt's central boiler system was later used in a Manchester industrial building.

The concept of utilizing vapor pressure as a means of activating a furnace was first introduced by William Powers in the year 1887. William Powers established the Powers Regulator Co. in Chicago, IL during the same year with the purpose of conducting research and advancing the field of thermostatic controls. The initial Powers thermostats were constructed from solid brass material and had a diameter of approximately 15 inches. In renowned structures such as the Chrysler and Empire State buildings, Powers heating systems were installed.

1.1.2. Bathwater Heater Development

Hot water is a necessity not only for central heating systems but also for domestic applications. The introduction of a closed-system gas bathwater heater marked the initial utilization of hot water in bathroom settings. The system, which was introduced in 1894, involves the heating of water through a gas flame as it traverses a sealed conduit, thereby avoiding exposure to noxious gases. This particular boiler enables the hygienic heating of water while preventing the condensation of combustion gases into liquid form. The regulation of water temperature is also feasible.

Although those appliances proved to be beneficial, their utilization necessitated a considerable amount of space in the designated areas. A wall-mounted water heater unit has been introduced to the market after a decade of development. This device enables the user to have access to additional space. However, it is imperative to note that a source of heat must be present in the same vicinity as the appliance.

1.1.3. Central Heating Development

In 1924, Vaillant innovated the development of a central heating boiler. Thus far, conventional heat sources such as stoves, ovens, and fireplaces have been utilized to provide warmth to individual rooms. This technological advancement enables the centralized heating of multiple rooms. Currently, it suffices to solely install radiators within the designated spaces. Due to the significant quantity of equipment, not all rooms in households could be effectively heated.

Central heating systems were not introduced until the 1950s. The initial central heating systems produced warmth by means of gas or oil boilers, which in turn heated the residence through radiators. The advent of electric heating in the latter part of the 20th century facilitated a more cost-effective and comfortable method of heating.

During the 1960s, a period characterized by significant challenges, opportunities, and innovations, Vaillant introduced the first wall-mounted gas-fired circulation water heater, known as the "Circo-Geyser MAG-C 20," to the market.

During the period 1962–63, Worcester Engineering unveiled the Firefly oil-fired boiler and, at the same time, served as a prominent provider of oil-fired central heating apparatus.

In 1967, Vaillant achieved the integration of heating and hot water functionalities into a single, space-saving, wall-mounted "Combi-Geyser VCW 20" boiler. The boiler demonstrated its effectiveness through its rapid heating capacity and adaptable thermal emissions. The Combi-Geyser VCW 20 represented a pioneering innovation by integrating both heating and hot water supply functionalities into a singular apparatus. The innovation in question is still being utilized by the industry in present times. The device exhibits noteworthy features such as rapid heating durations and the ability to adjust heat output in accordance with the required level.

1.2. Definition of Combi Boiler

A combi boiler is a device that integrates a central heating system with a domestic water heater. The system in question has the capability to function with a secondary heat source. Additionally, it can operate independently of a domestic unit, serving solely as a heating device. Furthermore, it has the potential to function as a hybrid system with the ability to be supplemented by electrical components. The utilization of natural gas combustion is a commonly employed technique for achieving the desired thermal energy output. Currently, investigations and practical examinations pertaining to hydrogen gas are underway with the aim of achieving the zero-carbon objectives established for the year 2030. The combi boiler can supply hot water to customers, which can be utilized in a closed circuit for central heating in radiators or for hot domestic water through the use of a plate heat exchanger.

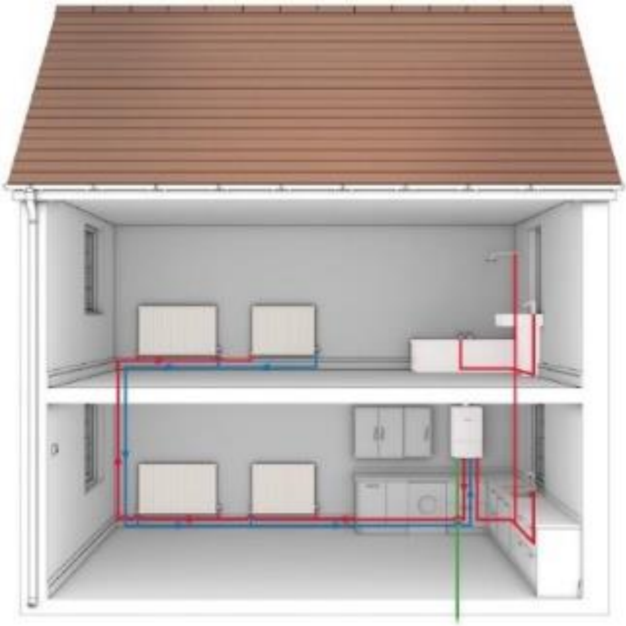

Figure 1.1. Combi Boiler System Illustration (worcester-bosch.co.uk, 2022)

The combi boiler runs in two different modes of operation. One of the available modes is the central heating mode. Water flows in CH mode under negative pressure generated by the hydraulic unit pump and passes through the heat cell. There are various categories of heat cells that are specifically designed to adapt to the diverse requirements of distinct boiler types. As a fundamental principle, the combustion process takes place between a modulated gas and a burner. Thermal energy is transferred through the primary heat exchanger. The process involves the circulation of water through the channels of a heat exchanger, resulting in an increase in temperature.

The process involves the circulation of hot water through the radiators. Heated radiators heat the building, and the water that is currently circulating in the radiator goes through a cooling phase. The combi unit receives the cold water, and the process continues in a cyclical manner.

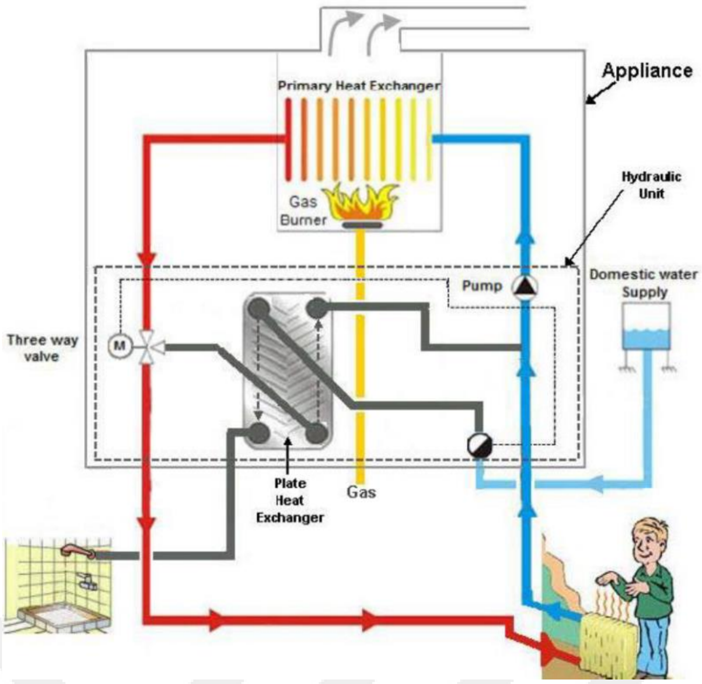

Figure 1.2. CH Cycle Working Principle (Gürler, 2018)

The second mode is related to the production of domestic hot water. In instances where there is a need for hot water from the tap. The hydraulic unit is subjected to the ingress of water. The flow of water is detected by the flow sensor, which triggers the rotation of the rotor and generates a corresponding signal. The signal is transmitted to the component known as the three-way valve. The 3-way valve initiates the domestic hot water channel while simultaneously terminating the central heating route. The domestic cold-water unit, consisting of various components such as a filter and PPD, arranges the flow of water towards the 3VW and DHW channels. The domestic water collected from 3WV is subjected to a heated plate heat exchanger (PHE), where it undergoes heat absorption. Subsequently, the heated water exits the primary heat exchanger (PHE) and is conveyed to the ultimate consumer for the purpose of facilitating daily hot water usage comfort. Compact plate heat exchangers are equipped with a pair of inlets. One of the inlets functions as a hot water inlet and is linked to the primary heat exchanger line. The heated water originating from the CH line is directed towards the Plate Heat Exchanger (PHE) through this specific location. Upon transferring its energy to the PHE, it subsequently reverts to the primary heat exchanger.

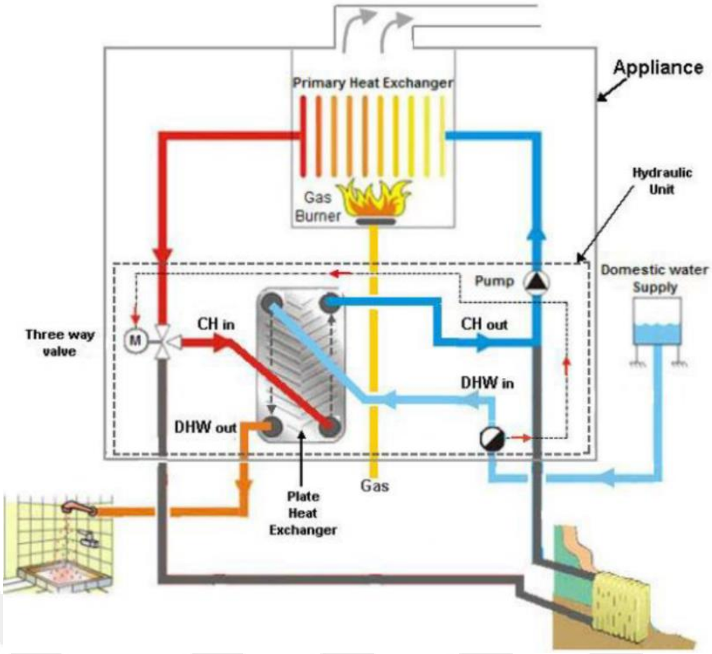

Figure 1.3. DHW Circle Working Principle (Gürler, 2018)

1.3. Brazed Compact Plate Heat Exchangers

Compact plate exchangers exhibit high heat performance capabilities, offer a diverse range of corrosion-resistant alloys, and possess a compact design. The utilization of larger plate heat exchangers (PHE) with gaskets is growing due to the drawbacks associated with the service and maintenance of brazed compact plate heat exchangers. The validity of heating efficiency status extends to compact plate heat exchangers, and the relationship between pressure drop and total heat transfer coefficient.

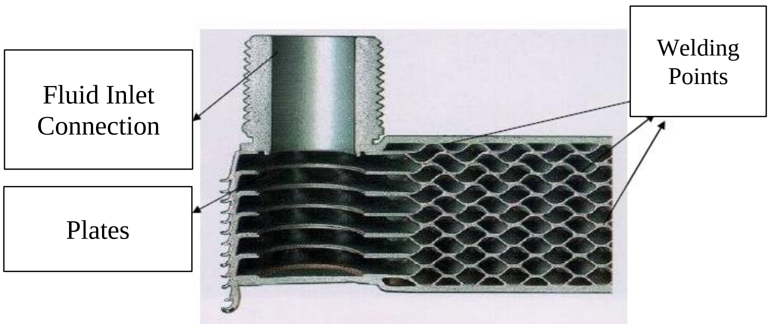

Figure 1.4. Cross section of Brazed Plate Heat Exchanger (Pekgüzelsu, 2015)

Brazed heat exchangers of a compact nature consist of interconnected channels that are joined through the process of brazing. The brazing process may involve the utilization of either nickel or copper as the brazing material. This enables the production of compact, simplified, and lightweight heat exchangers. The primary benefit of utilizing such a plate heat exchanger is the reduced manufacturing expenses in comparison to gasketed plate exchangers. The production methodology presents certain benefits; however, it also entails a drawback in the form of limited capacity to modify the plates or perform cleaning procedures. It is unfeasible to alter the quantity of plates utilized in compact plate heat exchangers. Compact plate exchanger cleaning is restricted but fluids in the C-PHE channels flows in high turbulence form. It is difficult to have dirt on the heat transferred surfaces (Yılmaz and Çomaklı, 1999).

Figure 1.5. Brazed Plate Heat Exchanger (Pekgüzelsu, 2015)

1.4. Working Range of Brazed Compact Plate Heat Exchangers

The operational scope of compact plate heat exchangers exceeds that of gasketed plate exchangers. Brazed-plate heat exchangers are known to be compact and efficient. Because they can be used in applications with temperature ranges from 160 °C to 232 °C, this type of plate heat exchanger is often used in industrial and refrigeration applications. This type of heat exchangers also has output range of 0.5 kW – 400 kW (Rafferty,2006).

1.5. Use Case of Brazed Compact Plate Heat Exchangers

Brazed heat exchangers are commonly utilized in cooling systems and heat pumps, serving as either an evaporator or condenser. Simultaneously, heated water can serve as a viable heat source for enclosed heating system circuits. This product has numerous industrial applications, particularly in the field of oil cooling. The utilization of nickel brazed plate heat exchangers has enabled the incorporation of this product in geothermal applications. The present investigation centers on brazed compact plate heat exchangers and their performance metrics in combi boiler applications.

Combi boilers consist of three primary modules. A primary heating unit, an expansion vessel, and a hydraulic system that contains the pump and facilitates the circulation of water through the combi appliance. Copper-brazed hydraulic module compact plate exchangers are currently being used in the context of domestic water heating applications. The component is equipped with a pair of inlet and outlet locations, totaling two each

The PHE receives heated water from the central heating system, which eventually flows through the internal channels and encounters the various components. The chilled water that has been cooled down is then returned to the pump for circulation. Simultaneously, the PHE receives cold water from the domestic supply. The plate heat exchanger (PHE) facilitates heat transfer through the circulation of water within its component channels, resulting in the heating of domestic cold water. The water is discharged from the system as domestic hot water at a temperature of 60 °C. Subsequently, the water is conveyed to the ultimate consumer for the intended purpose. The two distinct water circuits within the component remain separated during water flow, as the plates on the plate heat exchanger (PHE) are arranged in a manner that prevents their intermingling.

2. LITERATURE REVIEW

Akdari et al, showed that reliable thickness distribution predictions can be made with appropriate coupling plasticity and FE analysis in metal forming. The study utilized a multiscale modeling methodology to forecast the extent of thickness reduction in steel plate heat exchangers (PHEs) that are commonly employed in combi boilers. The successful integration of crystal plasticity and finite element analysis (FEA) enabled the accurate consideration of the functions of texture and microstructure. The utilization of crystal plasticity was employed to ascertain the appropriate multiaxial hardening rule for characterizing the material flow in the process of forming PHEs. This rule was subsequently integrated into the finite element (FE) metal-forming simulations. The present research indicates that accurate forecasts of thickness distribution can be achieved through the suitable integration of crystal plasticity and finite element analysis in the context of metal forming. The presented multiscale modeling approach serves as a significant framework for the development of novel PHEs that exhibit enhanced thermomechanical properties and decreased production expenses. (Akdari et al., 2015)

Gürler in his thesis investigated the mechanical behavior of the plate heat exchangers by applying tensile tests and FEA analysis to different PHE models which has different chevron angles at inside channels. The aim of this study is to employ numerical methods to examine the structural behavior of brazed-plate heat exchangers. Experimental methods were employed to determine the material properties of the brazing interface of plate heat exchangers for the purpose. Tensile and stress-based fatigue experiments have been conducted, resulting in the acquisition of material models. The validation of the material model utilized in numerical analysis has been conducted through explicit methodology, employing maximum displacement as a boundary condition. The present study examines the mechanical characteristics of brazed plate heat exchangers with a chevron configuration, with a particular focus on the influence of the chevron angle at varying pressure levels. (Gürler et al., 2018a)

Hayta in his thesis analyzed the fatigue behavior of the metals of plate heat exchangers that have been subjected to different materials. AISI 304L and AISI 316L materials were used in the study and were used efficiently in this thesis. This study examined the fatigue characteristics of plate heat exchangers (PHEs) fabricated with copper brazed AISI 316L and AISI 304L stainless steels. Strain-based fatigue tests were conducted to assess the viability of incorporating AISI 304L stainless steel in PHE manufacturing as a cost-saving measure.

Furthermore, a microstructural analysis was carried out on the brazed regions, and tensile tests were conducted on both the non-brazed and brazed steel specimens to ascertain the mechanical characteristics of the samples. The study conducted fatigue tests on twelve specimens for each sample group, utilizing four distinct load levels that were displacement (strain) controlled with a stress ratio of R = 0 and a frequency of 5 Hz. (Hayta et al., 2020)

Erdemir et al., have conducted a study which shows comparison of AISI 316L & AISI 304L stress corrosion resistances. The objective of this study was to investigate the feasibility of utilizing stainless steel types AISI 304L in place of AISI 316L for plate heat exchangers while maintaining their operational efficiencies and performances. The present study aimed to investigate the corrosion behavior of AISI 316L and AISI 304L stainless steel (SS) under simulated service conditions. The objective was to evaluate the feasibility of replacing AISI 316L SS with AISI 304L SS, which is known to be more cost-effective. The experimental parameters for plate heat exchangers included operating and boundary conditions such as temperature, pH, and chloride ion concentration of the solution. Electrochemical corrosion experiments were conducted to evaluate the pitting characteristics of the two stainless steel materials under simulated operating conditions and specific test parameters relevant to the types of pitting corrosion. (Erdemir et al., 2017.)

Sigvant et al., performed a simulation to observe the effect of different stamping die surface roughness on sheet metal forming which is first step for plate production with required design features. Over the past thirty years, the utilization of numerical simulation has progressively broadened its scope within the domain of sheet metal forming. The field of constitutive modeling is intricately linked to the advancement of computational tools for simulation purposes. This paper centers on the advancement of novel phenomenological yield criteria that have been formulated at the CERTETA research center. These criteria can characterize the anisotropic behavior of sheet metals. (Sigvant et al., 2019)

Jayahari et al., performed formability studies of austenitic stainless steel 304 and evaluate the friction factor for AI in deep drawing setup at elevated temperatures using LS-DYNA. The process of deep drawing entails the transformation of flat, thin sheet blanks into cup-shaped structures through sheet metal forming operations. The current demand for the formation of high-strength sheet metal and low-weight alloys under warm conditions is significant in various industries, including nuclear plants, cryogenic vessels, heat exchangers, and pharmaceuticals. The current study involves the deep drawing of austenitic stainless steel (ASS)-304 with varying blank diameters under warm conditions. The results indicate a noteworthy enhancement in the limitation of drawing ratio (LDR) from 2.16 at ambient temperature to 2.5 at a temperature of 150 °C, as evidenced by the determination of the drawn cups. (Jayahari et al., 2014)

Xu et al., have conducted a study with shell tube heat exchangers which is not directly related with compact plate heat exchangers shows that a failure analysis of stress corrosion cracking in heat exchanger tubes during start-up operation. This case can be similar in C-PHE's, and crack determination methods have been investigated. An analysis has been conducted on the failure of a newly installed heat exchanger during its initial start-up operation. By means of scrutinizing the operational chronicles of the machinery, scrutinizing the chemical compositions of tube material and corrosion products, and conducting metallographic examinations of specimens with cracks, the mode of cracking can be characterized as stress corrosion cracking (SCC) of austenitic stainless steel. Numerical calculation has demonstrated the existence of residual tensile stress resulting from seal expansion. (Xu et al., 2015)

Way et al., in their study gave significant information about brazing process and how it has been used effectively as a joining method for many years. Brazing has gained significant attention in recent times, owing to its potential to facilitate the development of various future technologies such as fusion energy, solid oxide fuel cells, and nanoelectronics. Additionally, brazing has been instrumental in advancing established fields like automotive light weighting by addressing the difficulties associated with joining aluminum to steel. The development of filler metals has played a crucial role in enabling these applications. The present review delves into the theoretical and practical aspects of brazing, with a specific focus on filler metals. Additionally, it provides an overview of the advancements made in the development of advanced filler metals and the potential opportunities that lie ahead. (Way et al., 2020).

Fedorov et al., investigated Nitrogen's effects on brazing atmospheres' effects on the hardness of the microstructural components of joints made of stainless steel. Nickel-based brazing fillers are frequently used in the production of stainless-steel components, such as heat exchangers utilized in energy and air-conditioning technologies. These components are typically manufactured in continuous furnaces or vacuum furnaces. The protective gas is frequently utilized to facilitate the brazing process in the continuous furnace. Nitrogen or nitrogen-hydrogen blends are frequently employed as protective gases. Nitrogen is frequently utilized as a cooling gas in the vacuum furnace. The mechanical properties of the microstructural constituents of brazed joints, particularly hardness, are affected by the nitrogen enrichment of both the braze metal and the base material. This study examines the impact of nitrogen enrichment on the hardness of microstructural components in joints, considering the process conditions. (Fedorov et al., 2019)

Hussaini et al., conducted a study and formability of AISI 316 at high temperatures is being investigated experimentally and numerically. The objective of this study is to examine the formability of austenitic stainless steel 316 under elevated temperatures. The formability of deep drawing can be evaluated based on the limiting drawing ratio and the thickness of the drawn cup. The current study involves the deep drawing of circular blanks at ambient temperature, 150 °C, and 300 °C, utilizing a 20-ton hydraulic press in conjunction with a furnace. Dynaform, in conjunction with the LS-Dyna solver, is utilized to conduct finite element simulations. (Hussaini et al., 2014)

Gatea et al., examined how process variables affect incremental sheet formation. The process of incremental sheet forming (ISF) is a recently developed method of flexible forming. The ISF process exhibits remarkable adaptability to traditional milling machines and necessitates minimal utilization of intricate tooling, dies, and forming presses, rendering it a cost-efficient and readily automatable technique for diverse applications. The objective of this manuscript is to furnish an exhaustive appraisal of the present-day cutting-edge of ISF procedures, encompassing their technological competencies and distinct constraints, while also delving into the ISF process parameters and their impact on ISF procedures. (Gatea et al., 2016)

Fukikoshi et al., examined on brazing copper to stainless steel using a brazing filler metal with a low silver content. The present study investigates the brazing process of copper to stainless steel (SUS304 JIS) utilizing a brazing filler metal with low silver content, Ag-50Cu, in the presence of an Ar gas atmosphere and a conventional furnace. The use of low-silver-content filler metals is considered economically advantageous. The present study aimed to investigate the brazing capability of a brazing filler metal with a low silver content when applied to copper and SUS304. A satisfactory joint was achieved, and a significant dissolution reaction took place at the copper interface. (Fukikoshi et al., 2014)

Persson conducted a numerical analysis of a BPHE for channel plate section which presents a methodology and steps needs to be taken for such investigation. This thesis addresses the topics of material thinning and formability for a specific sheet metal at a particular geometry. The investigation is conducted through physical experiments and finite element analysis. The physical experiments were subsequently compared with the finite element analysis to confirm or dispute the findings. (Björn Persson, 2011)

Bell et al., compared the pressure drop and heat transfer values with plate-fin heat exchanger. This study presents variable methods which can be used to investigation of air-side particulate fouling of microchannel heat exchangers. The present investigation involved the evaluation of the air-side pressure drop and heat transfer efficiency of plate-fin and microchannel coils in both uncontaminated and contaminated states. Two distinct types of dust, namely ASHRAE Standard Dust and Arizona Road Test Dust, were utilized to conduct tests on the heat exchangers. (Bell & Groll, 2011)

2.1. Material Selection

Compact plate heat exchangers commonly use copper brazing as well as the materials AISI 304L and AISI 316L. The primary distinguishing factor between AISI 304L and AISI 316L materials lies in the relative proportions of molybdenum and nickel present in their respective compositions. The optimal nickel ratio plays a crucial role in enhancing the capacity of masonry formation. Corrosion resistance is associated with the concentration of molybdenum. Corrosion resistance increases with an increase in the molybdenum ratio. Various tests are carried out to acquire empirical data and estimate the mechanical characteristics of substances.

2.1.1. Stress

When an object is subjected to external loads and is subsequently cut, a force distribution is present that maintains equilibrium among the various parts of the object. Stress is defined as the internal force magnitude at a specific point within the body. Stress is the limit value of the force per unit area as the field approaches zero. In this context, the entity under consideration is regarded as being both continuous and interconnected.

2.1.1.1. Normal Stress and Shear Stress

The normal stress, indicated by the symbol σ (Sigma), is defined as the magnitude of the force acting perpendicular to the unit area on the object.

$$\sigma = \frac{F}{A_0} \tag{1}$$

Assuming that the cross-sectional area c is composed of infinitesimal areas and that the force acting on this area is expressed as ΔFz, given that it is perpendicular to the area, the stated relationship can be formulated.

$$\Sigma z = \lim_{\Delta A \to 0} \frac{\Delta Fz}{\Delta A} \tag{2}$$

The study has neglected to consider the shear stress, which is defined as the force magnitude that acts tangentially to the cross-sectional area.

2.1.2. Tensile Testing

The application of tensile testing is a prevalent approach in determining the mechanical characteristics of materials employed in engineering applications. Tensile Testing machines can be electromechanical or hydraulics (Gürler, 2018). Following the addition of a constant at a specific location, the test specimen undergoes a tensile force from a distinct point. The application of this force continues until the material experiences rupture. The graph representing the material is generated by recording the extent of elongation that transpires in the direction of the exerted force. The diagram is commonly referred to as a stress-strain diagram, and it is typically characterized in two distinct manners.

2.1.2.1. Conventional Stress-Strain Diagram

The calculation of the nominal or engineering stress involves the division of the applied load *P* by the initial vertical cross-sectional area of the sample A0. The calculation assumes constancy across the cross-sectional area and along the gauge length.

$$\sigma = \frac{P}{\mathrm{A}_0} \tag{3}$$

The nominal or engineering unit elongation can be determined by directly reading the strain gage, or alternatively, by dividing the elongation of the sample L0 by its initial length to obtain the change in the master length of the sample. The assumption of constant strain within the region between the reference points leads to the derivation of the specified equation.

$$\in = \frac{\Delta L}{L0} \quad (4)$$

The conventional stress-strain diagram is obtained by plotting stress on the vertical axis and strain on the horizontal axis, where the values of σ and ∈ are emphasized. It is important to note that while the diagram derived from two distinct samples of a particular material may exhibit a high degree of similarity, it will invariably possess some degree of dissimilarity. The outcomes are contingent upon factors such as the material's composition, microscopic imperfections, production technique, loading velocity, and experimental temperature. The curve exhibits four distinct behaviors based on the degree of elongation exhibited by the material.

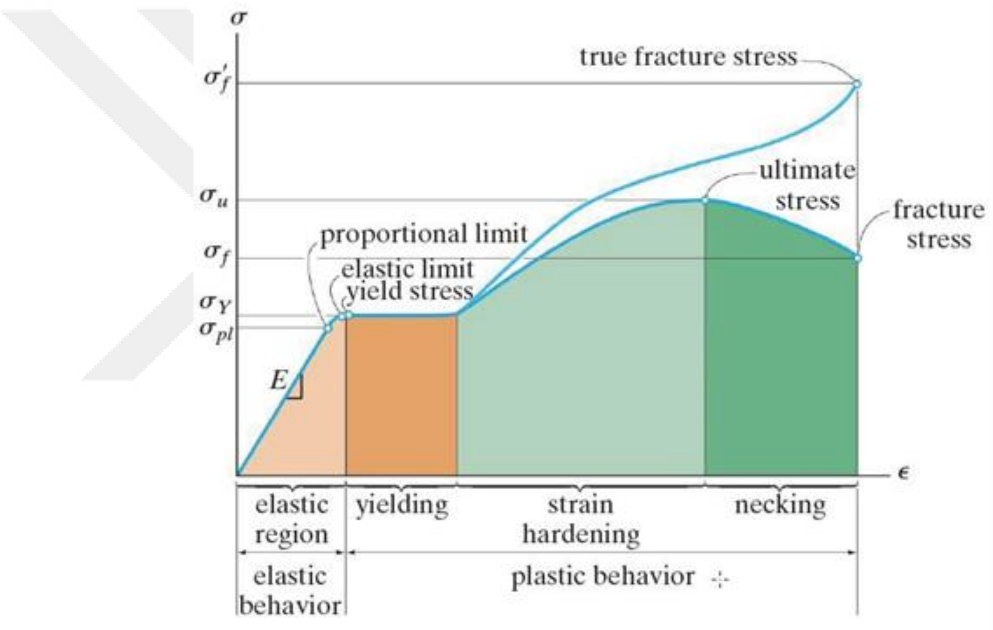

Figure 2.1. Engineering and true stress-strain diagram for ductile materials (Hibbeler, 2016)

2.1.2.1.1. Elastic Behavior

The graph depicted exhibits a linear relationship where stress and strain are directly proportional throughout most of this domain. The substance that exhibits such behavior is referred to as linear elastic in the field of materials science. The point at which a linear correlation reaches its maximum voltage is referred to as the proportionality limit σpI.

2.1.2.1.2. Yielding

The material is subjected to an increased applied force to induce elongation of the specimen. Once the stress level surpasses a critical threshold, the elastic deformation will become permanent and irreversible plastic deformation will commence. The point or localized area in a material where it exhibits a significant deviation from its elastic behavior and undergoes plastic deformation can be referred to as the yield point or yield strength of the material, denoted as σy. The yield stress and strain to yield are respectively defined as the stress and strain values at which yielding occurs. The occurrence of the yield point is observable in certain engineering materials, such as low-carbon steel, while it may not be noticeable in other types of engineering materials, such as certain steels and materials based on polymers.

2.1.2.1.3. Necking

The uniform deformation of a tensile specimen persists until the applied force attains a critical value upon application of a load that induces the ultimate tensile stress on the material, the cross-sectional area of the sample will commence to decrease in a localized region of the specimen, as depicted in the Figure 7. The constricted portion of the curve is commonly referred to as necking.

2.1.3. Tensile Test Results of AISI 316L Stainless Steel

The modulus of elasticity is determined through the conduction of tensile tests on a sample prepared from sheet material with a thickness of 0.3 mm, while ensuring that the elastic deformation limits were not exceeded. The measurement of elongation during elastic loads is carried out with precision using a macro extensometer, as depicted in Figure 7.

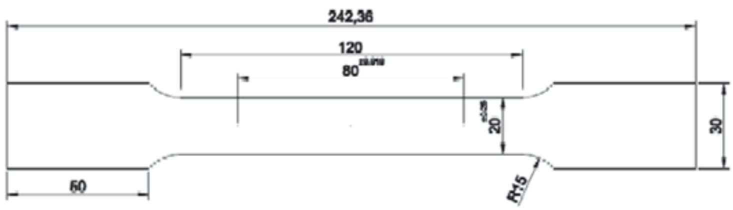

Figure 2.2. Standard flat tensile specimen (Atılım Universty, 2016)

Figure 2.3. Macro extensometer (Atılım University, 2016)

The determination of the modulus of elasticity in AISI 316L stainless steel sheets also considers the rolling directions. Each sample was subjected to five repetitions of the tests during this experiment. Table 2 displays the average values of the modulus of elasticity pertaining to each rolling direction.

Table 1. The average modulus of elasticity values is presented for each direction of deformation and the plastic flow curve for AISI 316L stainless steel is depicted in Figure 9.

Material	**Thickness (mm)**	**Rolling direction (°)**	**Young's Modulus (GPa)**	**Standard deviation**
AISI 316L	0.3	0	190	+ / - 1.10 GPa
		45	189	+ / - 0.78 GPa
		90	197	+ / - 0.37 GPa

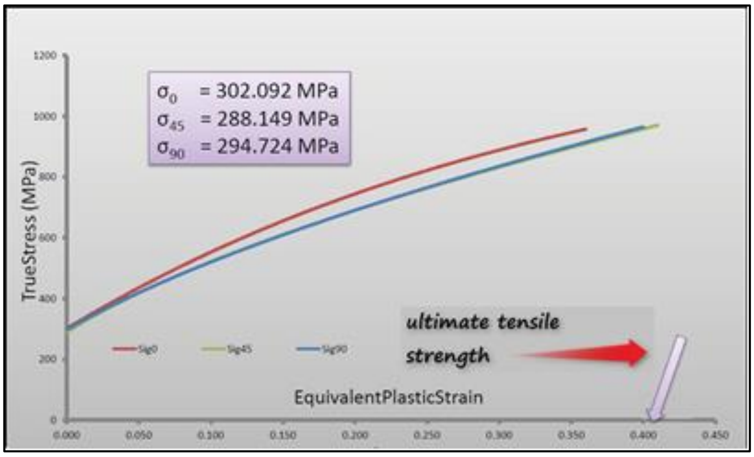

Figure 2.4. Plastic flow curve of AISI 316L stainless steel (Gürler, 2018)

A comparable methodology was utilized by R.K. Blanford et al., in the examination of 144 distinct specimens. The study involved the application of AISI 304L and AISI 316L materials in a tensile test, with the subsequent documentation of the findings.

2.2. Construction and Materials

The Brazed Plate Heat Exchanger is a condensed device that comprises of corrugated plates made of stainless steel, which are joined together through the process of brazing, utilizing copper and nickel. Plate packages, both front and rear, are frequently designed to create a self-contained unit by means of sealing.

The thermal efficiency and hydraulic performance of the BPHE unit are determined by the distinct corrugation pattern present on each plate. Furthermore, it is worth noting that a total of four to six apertures are strategically incorporated into the corners or edges of said plates. The input and outlet port manifolds for the various process fluid circuits are formed by the arrangement of alternating plates at a 180° angle to each other. A single plate is created by the joining of two channel plates, which is employed in scenarios where rapid identification of leaks and prevention of cross-contamination are of utmost importance.

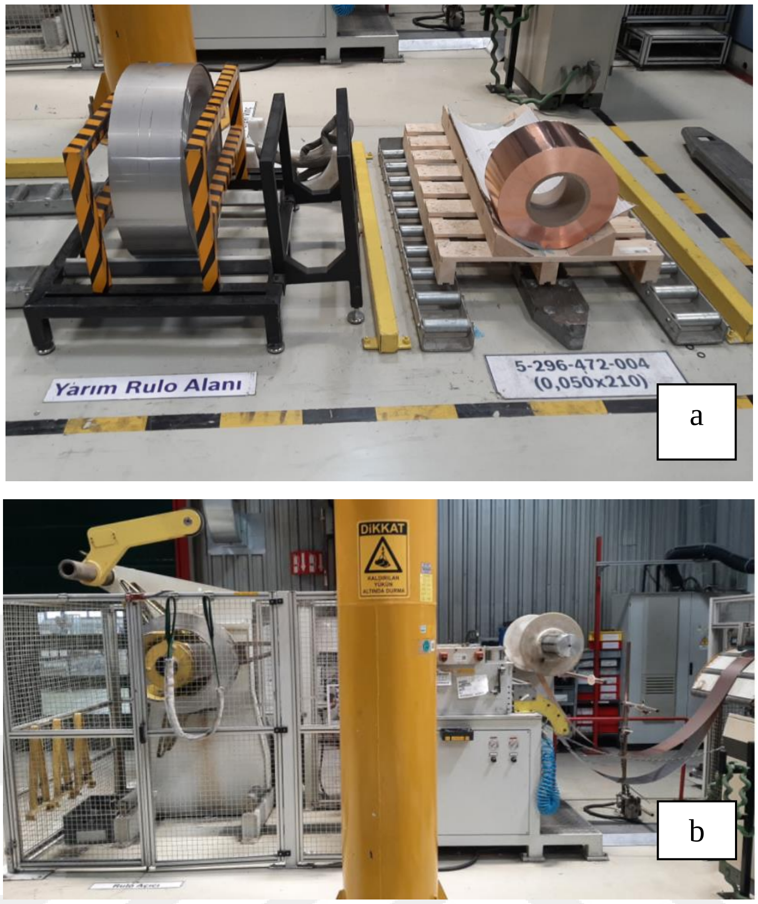

Figure 2.5. Decoiling (a) / Sheet Material Feeding Process (b)

During the manufacturing process, plate packs are created by simultaneously chopping and packing stainless steel and brazing material that are fed from their respective coils. The packs, in conjunction with supplementary elements such as distribution rings, blind rings, and other related components, are constructed with the requisite cover plates and connectors. The plates, which are generally made of stainless steel and re compressed to the body in series, form the main backbone of the heat exchanger. (Şahin M, 2021).

The brazing procedure of the plate package involves the utilization of capillary forces to facilitate the movement of the filler or brazing material towards the contact points that exist between the alternating plates, thereby creating braze connections. The utilization of braze connectors substantially improves the structural robustness of the BPHE modules, rendering them suitable for operational pressures of up to 30 - 45 bar.

The stacked units, which are either filled with dead weights or spring-loaded weights, undergo a vacuum brazing process for approximately eight hours within furnaces. Advancements in the production of brazed plate heat exchangers are being made through the refinement of brazing techniques, exploration of alternative brazing materials, and the optimization of raw material shapes for brazing materials. Plate heat exchangers produced by high heat and vacuum application on the plate connection points of copper or nickel welding material. (Shah and Sekulic, 2003).

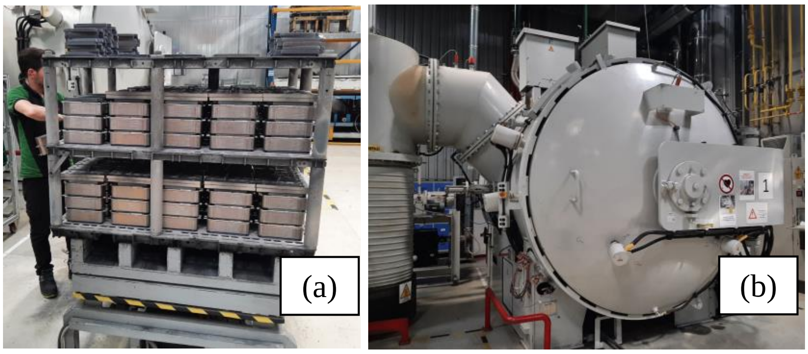

Figure 2.6. Weight Stacking (a) / Vacuum Brazing (b)

The placement of different types of connections on the front or rear face can be determined based on the specific requirements of the market and application. Blind rings and supplementary sealing plates are commonly employed to isolate cover plates from channel plates. The variability of the cover plates' dimensions and quantity is contingent upon their intended application. Furthermore, the guidelines for the installation of the heat exchangers are provided.

It is imperative to identify both the quantity and positioning of interconnected channels for a specific process fluid stream. The typical construction material for standard BPHEs is AISI 316 (AISI 316L) and AISI 304 (AISI 304L) steel, which is joined using copper brazing material. These BPHEs are designed to withstand pressures of approximately 31 bar. Nickel is employed as a brazing agent in situations where the incompatibility of copper with process fluids precludes its utilization.

2.3. Plate Design

A heat exchanger is a device that provides energy transfer between two fluids at different temperatures. (Erdinç, 2019) The thermal and hydraulic characteristics of the plate heat exchanger are predominantly determined by the geometric parameters that are incorporated in the corrugated plate design. Numerous scholars have conducted research and documented the impact of geometric variables, including the chevron angle (which represents half of the included angle of the corrugation pattern with respect to the main flow direction), corrugation pitch and depth, plate thickness, port aperture dimensions and location, plate aspect ratio, and other factors, on the efficacy of plate heat exchangers.

Mustafa Sevim designed 6 different basic PHE types with different design features and flow configurations in his study. He evaluated the effects of different chevron angles with numerical and theoretical approach. (Sevim M, 2016.)

The augmentation of heat transfer and pressure drop is commonly observed with an increase in chevron angle, which can be attributed to the intensified flow interactions and enhanced degree of barrier separation within each channel.

The spacing of grooves has an impact on the separation of flow boundaries and the resistance of flow in both the transverse and longitudinal directions. The impact of the depth of a plate on various factors, including but not limited to boundary separation, effective hydraulic diameter, and the number, size, and shape of brazed connections, is noteworthy.

The design of port apertures and their placement is typically aimed at achieving a low pressure drop, efficient distribution in channel/port manifolds, and adequate structural integrity.

Elevated plate aspect ratios are distinguished by a heightened level of counter current flow, albeit with a concomitant rise in pressure drop.

The persistent need to enhance the efficacy of thermal and hydraulic systems, broaden their operational ranges, accommodate novel applications, and comply with regulatory frameworks governing the nature and volume of process fluids has spurred the creation of alternative plate configurations that are customized to the flow dynamics and process variables of particular use cases. Several manufacturers provide comprehensive information about their designs on their websites and product sheets.

2.4. Analysis of Plate Heat Exchanger

Gullapalli clarified diverse techniques for evaluating the performance of compact brazed plate heat exchangers (BPHE) in a range of applications, including single-phase, condenser, evaporator, cascaded, and transcritical operations. These techniques are crucial in the advancement of heat exchanger selection software and in the estimation of geometry parameters in the process of developing new products. Also, relevant calculation steps required for C-PHE performance evaluation has been mentioned and briefly discussed. (Gullapalli, V, 2013) Based on his work in this study, similar methods were used for definition and calculation of performance parameters of compact brazed heat exchangers.

It is related to the mass flow rate specific heat capacity and the temperature difference between inlet and outlet.

$$Q = mCp\Delta T \tag{6}$$

$Q = m_h C_{ph} \Delta T_h$ Heat discharged from hot fluid. (7)

$Q = m_c C_{pc} \Delta T_c$ Heat absorbed by cold fluid. (8)

Logarithmic mean temperature difference is:

$$\Delta T_{lm} = \frac{\Delta T_1 - \Delta T_2}{\ln \frac{\Delta T_1}{\Delta T_2}} \tag{9}$$

$$\Delta T_1 = T_{h1} - T_{c2} \tag{10}$$

$$\Delta T_2 = T_{h2} - T_{c1} \tag{11}$$

2.4.1. Governing Parameters and Calculation Procedure

Total heat transfer area of a plate given by:

$$A_1 = \Phi \, x \, A_{1p} \tag{12}$$

The enlargement factor is given by equation. It generally lies between 1.15 < Φ < 1.25. A_{1p} is:

$$A_{1p} = L_p . L_w \tag{13}$$

L_p & L_w can be estimated from the port distance L_v & L_h and port diameter D_p are given as below.

$$L_p = L_v - D_p \tag{14}$$

$$L_w = L_h + D_p \tag{15}$$

The mean channel spacing (b) can be taken as the difference between plate pitch (p) and plate thickness (t) thus,

$$b = p - t \tag{16}$$

$$p = \frac{L_c}{N_t} \tag{17}$$

Diameter of the channel, De, is defined as:

$$D_e = \frac{4 \mathrm{x} b \mathrm{x} L_w}{2(b + L_w \Phi)} \sim \frac{2b}{\Phi} \tag{18}$$

2.4.2. Single-Phase Heat Transfer

Heat transfer correlation is in the form:

$$Nu=C_1(Re)^m(Pr)^{1/3}(\frac{\mu_b}{\mu_w})^{0.17} \quad (19)$$

C_1 and m values obtained from literature. The Reynolds number, Re based on channel mass velocity and equivalent diameter, D_e, of the channel is defined as:

$$Re = \frac{G_C D_e}{\mu} \quad (20)$$

Where, G_c = channel mass velocity which is given by:

$$G_c = \frac{\dot{m}}{N_{Cp} b l_W} \quad (21)$$

and N_{Cp} is the number of channel plates per pass and obtained by following equation.

$$N_{Cp} = \frac{N_t - 1}{2N_p} \quad (22)$$

2.4.3. Pressure Drop

Total pressure drop is combination of frictional channel pressure drop Δp_C and the port pressure drop Δp_p.

The channel pressure drop is given by equation:

$$\Delta p_C = \frac{4 f L_{\text{eff}} N_p}{D_e} \frac{{G_c}^2}{2p} (\frac{\mu_b}{\mu_w})^{0.17} \quad (23)$$

The friction factor (f) in the equation 23 is given by:

$$f = \frac{C_2}{Re^p} \quad (24)$$

$C_2$and p values are taken from literature. The pressure drops in the port ducts Δp_p, can be roughly estimated as 1.4 velocity head.

$$\Delta p_p = 1.4 N_p \frac{{G_p}^2}{2p} \quad (25)$$

$$G_p = \frac{\dot{m}}{\frac{\pi {D_p}^2}{4}} \quad (26)$$

For total pressure drop:

$$\Delta p_t = \Delta p_C + \Delta p_p \quad (27)$$

The overall hear transfer coefficient is:

$$\frac{1}{U_c} = \frac{1}{h_h} + \frac{1}{h_c} + \frac{1}{k_w} \quad (28)$$

And under fouling conditions (fouled or service overall heat transfer coefficient):

$$\frac{1}{U_f} = \frac{1}{h_h} + \frac{1}{h_c} + \frac{1}{k_w} + R_{fh} + R_{fc} \quad (29)$$

The relation between U_c & fouled U_f, and cleanliness factor, CF, can be written as:

$$U_f = U_c(CF) = \frac{1}{\frac{1}{U_c} + R_{fh} + R_{fc}} \quad (30)$$

The heat balance relations in PHE are the same as for tubular heat exchangers. The required heat duty. Q_r, for cold and hot streams is obtained from equations 7 and 8.

On the other hand, actual obtained heat duty for fouled conditions is defined as:

$$Q_f = U_f A_e F \Delta T_{lm} \quad (31)$$

A comparison between $Q_r$and Q_f defines the safety factor, C_s of the design:

$$C_s = \frac{Q_f}{Q_r} \quad (32)$$

2.4.4. Thermal Performance

Heat exchanger has some heat transfer equations resulting in the following dimensionless groups.

Heat capacity ratio:

$$C' = \frac{C_{min}}{C_{max}} \quad (33)$$

Where C_{min} is smaller magnitude of C_h and C_{max} is the larger value of C_C.

A possible method to increase the heat transfer performance for single phase internal flow is to use utilize curved channels instead of straight channels. Büyükasik in his study completed set of calculations and claimed the new innovative plate which is used in plate heat exchanger is more efficient than some geometries in literature. (Büyükasik. 2020.)

2.4.4.1. Heat transfer effectiveness

Effectiveness of heat transfer rate can be described as ratio of actual heat transfer rate to the time of dynamically limited maximum possible heat transfer rate.

$$\mathcal{E} = \frac{Q_{actual}}{Q_{max}} \quad (34)$$

Actual heat transfer rate can be found from energy rejected by the hot fluid or energy absorbed by the cold fluid from equations (2) and (3).

Therefore, maximum possible heat transfer can be calculated from:

$$Q_{max} = (\dot{m}c_p)_C(T_{h1} - T_{c1}) \text{ if } C_C < C_h \quad (35)$$

$$Q_{max} = (\dot{m}c_p)_C(T_{h1} - T_{c1}) \text{ if } C_h < C_c \quad (36)$$

Since the fluid that might undergo the maximum temperature difference is the flute with the minimum heat capacity rate C_{min}.

There are possible ways to increase the heat transfer in heat exchanger such as chevron angle optimization and usage of nano liquid usage between plates. Peker in her study investigated the effects of geometries, flow rates and concentration ratios of used values. With increase of turbulent density total heat transfer rate and effectiveness of plate heat exchanger increases. (Peker G, 2021)

Nanofluids provide a significant performance increase in various energy applications, both in heat storage and heat absorption. (Hacısalihoğlu, 2021)

With high heat conduction rates of nanofluids, it is now possible to increase the effectiveness of the heat transfer equipment. (Khanlari, 2018) Also plate thickness is an effective parameter on heat exchanger efficiency. The thinner the plate thickness, the more efficient and stable the heat transfer, and better the process control. (Kocabaş, 2014)

2.5. Finite Element Analysis (FEA)

The finite element analysis technique has been devised to address engineering problems that are beyond the scope of analytical methods. The mechanics of materials and theory of elasticity can be employed to derive stress and strain distributions for curved beam problems. However, the analytical approach may not be as effective or robust for intricate geometries, such as those found in car suspension systems or airplane wings. Initially, the approach is employed to compute the stresses and strains experienced by engineering components when subjected to external loads.The finite element method can be utilized to anticipate the physical behavior of mechanically designed components prior to the commencement of fabrication.

One crucial aspect in determining the structural behavior of a product through finite element analysis is the validation of the numerical solution using experimental techniques. The purpose of this is to guarantee the appeal of the outcome, as well as to optimize cost efficiency in the production procedure. The advancement of the finite element method (FEM) has been expedited in tandem with the technological enhancements in computing.

The Finite Element Method (FEM) involves partitioning a given structure into multiple elements to calculate desired outputs such as displacement, strain, or stress. These segmented elements are subsequently reassembled at designated 'nodes'.

The process of discretization, also known as meshing, is utilized in this context. The various shapes of elements can be observed in one, two, or three dimensions.

Nodes represent the degrees of freedom, which refer to the independent movements that are possible. The nodes' behavior has been established using equilibrium equations, and their mathematical representation has been expressed in the form of algebraic equations in matrix notation. The finite element method involves the systematic formulation of individual equations, which are subsequently combined to encompass the entire domain. The outcomes of the finite element analysis entail the computation of the displacements at every node and the generation of stresses within each element.

2.5.1. General Steps of Finite Element Method

The behavior of physical phenomena is contingent upon the intricacy of geometry, the specified initial and boundary conditions, and the material properties of said geometry. When dealing with intricate geometry, boundary conditions, and material properties in engineering systems, obtaining an analytical solution for the corresponding differential equation that represents the problem can prove to be a challenging task. The finite element method is commonly employed to solve mathematical descriptions of various engineering problems encountered in practical applications.

The finite element method is a systematic approach to solving continuum problems that involves a sequential and structured procedure. The methodology for obtaining numerical solutions to engineering problems is outlined as follows:

i) Discretization

The initial stage of finite element analysis involves the identification of an appropriate element type through the partitioning of the solution domain into finite elements. The variation in element type utilized in analysis software has a direct impact on the convergence and sensitivity of the solution. The one dimensional (1D), two dimensional (2D) and three-dimensional elements (3D) can be used in finite element analysis as can be seen in Figure 12.

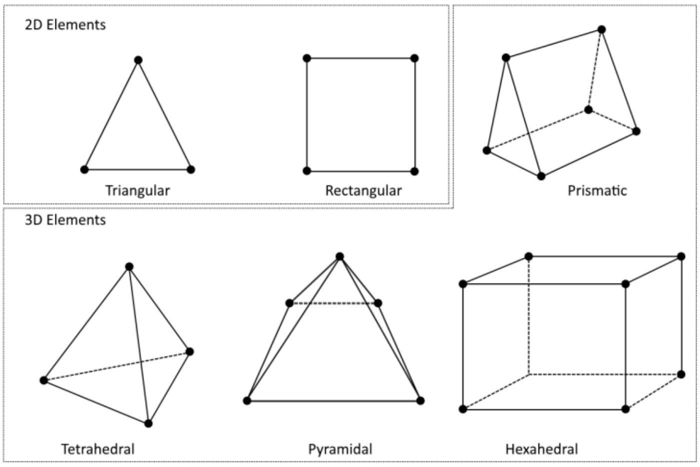

Figure 2.7. Representation of 1D, 2D and 3D element types (Comsol, 2017)

ii) The definition of interpolation functions pertains to the utilization of polynomial functions as the preferred type for interpolation. The polynomial function's degree is determined by the quantity of nodes present in a singular element.

iii) The identification of element properties can be achieved through the utilization of the variational approach and Galerkin's method, which are the most suitable algorithms for the establishment of the governing matrix equation.

iv) The fourth step in the procedure pertains to the assembly of discretized elements for the purpose of achieving a global solution through the formulation of element equations. Prior to solving a problem, it is crucial to establish the boundary conditions and material properties.

v) Post-processing is the final stage of the procedure, wherein the data obtained from a numerically solved engineering problem is processed to present the analysis output in terms of established metrics, such as principal stresses and strains.

2.5.2. Finite Element Analysis by Using ANSYS

ANSYS is a commonly utilized software for finite element analysis, which is employed to ascertain the physical characteristics of engineering systems. The initial iteration of the ANSYS numerical solution methodology was developed in the early stages of 1976. The ANSYS concept's developmental process commenced by generating solutions for problems of one and two dimensions. Currently, ANSYS is utilized for a wide range of engineering predicaments that exhibit intricate geometry and boundary conditions. These include but are not limited to fatigue analysis, cooling analysis of nuclear power plants, and biomedical applications.

The present thesis employs the Workbench module of ANSYS software to forecast the structural performance of a chevron type brazed plate heat exchanger under its operational circumstances. The outcomes are assessed through static structural analysis.

Furthermore, the evaluation of fatigue in the numerically analyzed geometry was conducted utilizing the static structural outcomes of the software. The following section outlines the modeling procedure and ANSYS specifications.

In the context of linear structural analysis, the solution for the global displacement vector is obtained through a matrix equation, as depicted in Equation (37).

$$[K] \cdot \{x\} = \{F\} \tag{37}$$

Classes of structures that are of great importance exhibit a non-linear correlation between force and displacement, as depicted in Figure 13. Structures that exhibit a non-linear relationship between F and u (x) are commonly referred to as non-linear structures. This is since the plot of F versus u (x) for such structures does not follow a straight line.

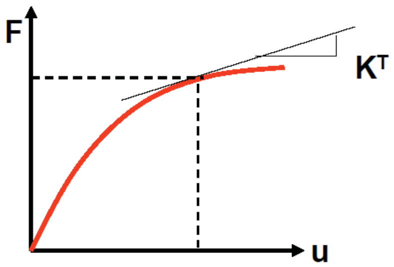

Figure 2.8. Force vs displacement (ANSYS Inc., 2016)

A structure can be classified as nonlinear when the application of a load results in substantial alterations in its stiffness. Common causes for alterations in stiffness include exceeding the elastic limit resulting in plastic deformation, significant deformations in the geometry, and alterations in the contact status between two bodies.

The presence of nonlinearities can be attributed to three primary sources, namely geometrical, material, and contact. Nonlinear analysis involves the inability to predict the structural response through a set of linear equations.

Nonlinear structures can be analyzed through an iterative process of linear approximations along with necessary corrections. The iterative process known as the Newton Raphson method is utilized in the Mechanical module of ANSYS Workbench.

The present thesis employs a modelling methodology that incorporates two primary sources of nonlinearity, namely, geometry-based large deflection and plasticity modelling. The activation of large deflection is attributed to the high-pressure loading, and the material has been characterized using a multilinear kinematic hardening model to depict the plastic deformation behavior.

3. MATERIAL – METHOD

3.1. Material

This study investigates the relationship between top plate material and performance parameters for compact brazed heat exchangers. Aim of this study is to find suitable alternative materials and decrease the cost of the product by keeping the desired output levels.

Material selection process has been completed with considering parameters related with formability, brazing capability, corrosion resistance, dynamic resistance of the material and overall cost. AISI 316L used top plate thickness reduced from 1 mm to 0.5 mm and current material have been changed from AISI 316L to AISI 304L. PHE top plates have been produced with AISI 316L 1 mm, AISI 316L 0.5 mm and AISI 304L 0.5 mm thicknesses. In total, three different top plates and different behaviors in the system level have been evaluated in this thesis.

3.2. Method

The plate heat exchangers were manufactured using AISI 304L and AISI 316L 0.5 mm top plates. Subsequently, the produced heat exchangers underwent initial functional testing. The test results yielded positive outcomes, and the corresponding output values were assessed. The products underwent a pressurization test, commonly referred to as a burst test, to assess and analyze their mechanical strength thresholds. The plate heat exchanger fabricated using a 316L 0.5 mm top plate exhibited deformation at a pressure of 24 bar, whereas the plate heat exchanger fabricated using a 304L 0.5 mm top plate experienced deformation at a pressure of 16 bar. Burst performance tests have been applied at 36 bar to observe the top plate material deformation and internal leakage status by exceeding the recommended test pressure value of 15 bar which is maximum working pressure (10 bar) times factor of safety value (1.5) defined in section 6.2.1.1. of BS EN 625:1996 Gas-fired central heating boilers – Specific requirements for the domestic hot combination boilers of nominal heat input not exceeding 70kW.

The numerical method configuration for FEM has been established using ANSYS. The necessary data pertaining to materials has been imported. The initial and boundary conditions have been defined. The prescribed testing protocols have been clarified, and the conditions for assembly have been clarified. FEM software package has been implemented and verified through comparison with relevant experimental data. The present investigation employs both experimental and numerical techniques to establish a correlation between the type of material utilized and the performance of burst testing. Findings have been evaluated and reported.

Table 3.1. Operation conditions of C-PHE according to EN625

Description	Unit	Specifications		
		Nom	Min	Max
DHW IN Temperatures	°C	10	1	30
CH IN Temperatures	°C		1	95
DHW Static Pressure	bar	2	0.2	10
CH Static Pressure (Class II acc. to EN15502)	bar	3	-	4.5
CH Static Pressure (Class III acc. to EN15502)	bar	4.5	-	9

3.2.1. Burst Test Description

1-) The test piece is attached to the apparatus.

2-) Samples to be tested; It is supported by the appropriate block according to the number of plates and connected to the apparatus.

3-) The samples to be tested are fixed to the places shown in the Figure 14, with the holes facing down, using the support apparatus on the test stand.

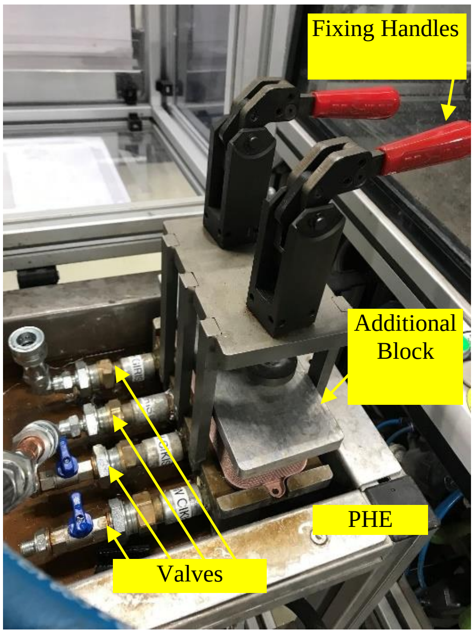

Figure 3.1. PHE Holding Stand

4-) The valve details and sample position are made as shown in the Figure 15.

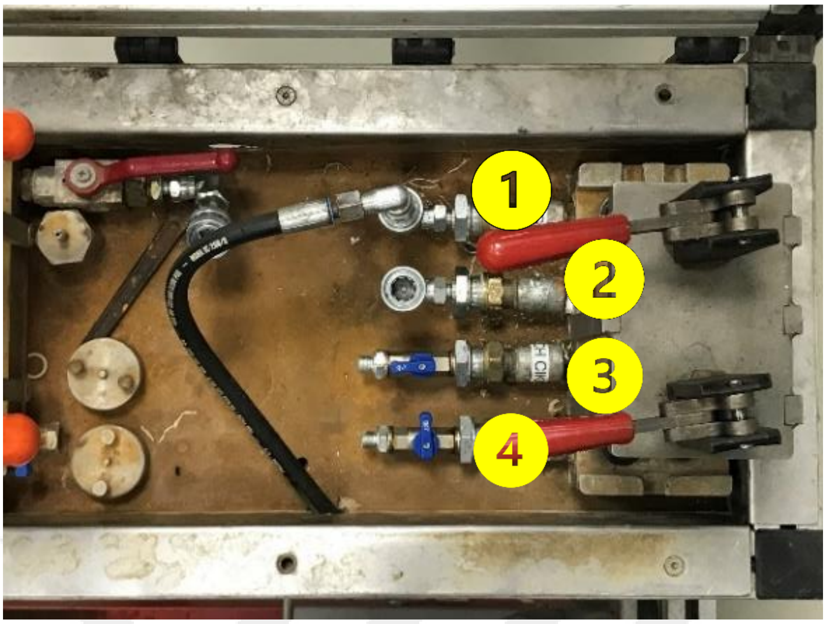

Figure 3.2. Burst Test Stand Port and Valve Details

Valves 1 and 4 are used for CH line pressurizing in the PHE which is not needed for domestic line pressure test. To increase the pressure in the domestic line pipe that is connected to valve 2. The valve must be opened during the initiation phase of the test. The initial opening of valve 3 serves the purpose of preventing the entrapment of air within the sample under examination. The valve is closed after confirming the absence of air in the preceding tested sample, while the water is in motion.

The valve 4, which permits the assessment of potential leaks in the test samples, should consistently remain open. The CH line and Domestic line are distinct sections within the PHE system, and it is imperative that these two fluids remain separate and should not be mixed. At elevated pressures, it is anticipated that the brazing points, which serve as the interconnection points between the CH and DCW lines, will take damage. This phenomenon results in the impairment of the functionality of the components due pressure drop.

Afterwards, the impermeable mica glass cover, designed to withstand water pressure, is securely sealed on the test apparatus. The following procedure involves adjusting the apparatus to the intended pressure level.

5-) Water is pressed from the pump at the specified pressures

Table 3.2. Load Profile of Applied Burst Test

Applied Pressure (bar)	Time under pressure (min)	Checkpoint
6	3	It is visually checked whether there is a pressure loss on the manometer clock pointer and whether there is water leakage in the heat exchanger. This valve 4, which allows us to understand whether there is a leak in the test sample, should always be open. If water is coming, it means there is a leak.
12	3	
18	3	
24	3	
30	3	
36	3	

6-) If there is no water leakage, the pressurizer valves are slowly loosened. Then, the closed valves numbered 1 and 3 are opened slightly to discharge the water pressed into the heat exchanger.

7-) C-PHE is removed from the test apparatus and visually checked for swelling and deformation at the top and bottom of the heat exchanger.

3.2.2. Maximator Hydraulic Power Pack Used Burst Test

Maximator pressurizer equipment preferred because of its controllable load application capability. Also, with this equipment it is possible to reach up 200 bar testing pressure. Although, 120 bar maximum usage is suggested for safety reasons. With this unit pressure increment was more precise and 1bar increment was possible. This makes it possible to have better observation during the test and create the boundary conditions needed for simulation.

3.2.2.1. Maximator Test Kit Components

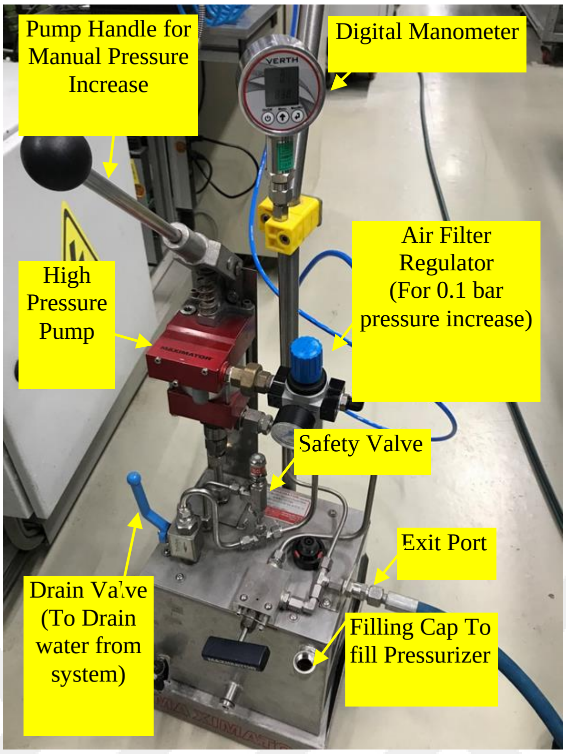

Figure 3.3. Maximator Sub-Components.

3.2.2.2. Maximator Burst Test Description

1-) Connect the Maximator air connection to the regulator first and then to the mains.

2-) Maximator and parts are connected.

3-) Water level is checked.

4-) The air in the part is expelled.

5-) If any, the inlets, and outlets of the test pieces are closed.

6-) The outlet valve is set to the open position to continuously pressurize.

7-) The test piece is put into the cage.

8-) If the discharge valve is open, it is turned off.

9-) The manometer opens and the high-pressure value, if any, is reset.

10-) If desired, rapid pressurization can be done with the air filter regulator at first, or it can be pressurized manually with a high-pressure pump if desired.

11-) Pressurization should not exceed 200 bar.

12-) Compression is stopped when the desired pressure value is reached.

13-) The relief valve is opened.

14-) When the manometer reads 0, the test piece is removed from the cage.

15-) Test piece connections are disconnected.

16-) The manometer is turned off.

17-) The air connection is first disconnected from the mains and then from the Maximator.

3.2.2.3. Operating Conditions and Test Setup

Number of EUT: 12 (6 EUTs 1 mm Top plate thickness, 6 EUTs 0.5 mm top plate thickness)

Medium : Water

Temperature : Ambient

Pressure : Increased until leakage occurs

Assembly Position : EUTs assembled in mould to prevent any leakage at high pressures.

Measurement Point : EUTs are observed for any water leakage during tests

3.2.3. Functional Test of AISI 304L 0.5 mm Top Plate Used PHE

For functional test, top plates with AISI 304L and AISI 316L material have been used. Aim was to validate if samples are aligning with relevant output performance levels. Tests were performed with AISI 304L used C-PHEs that have 26, 24 and 20 number of plates. 3 samples of each were tested. Acceptance criteria of this test was to fulfill minimum and maximum range of heat output and DHW temperature requirements for each plate numbers.

3.2.3.1. Functional Test Description

i) Water from previous experiment to be drained. C-PHE to be connected to test platform,

ii) Relevant valve to be opened, Combi starts, TPM to be completed,

iii) Bypass lines and central heating lines to be opened. Pressure to be increased 2.5 bar - 2.8 bar

iv) Water circulation on CH line to be continued until the temperature on Pt 3 reaches the 78˚C

v) Close the valves and pump and end the CH circle. Cool the heated PHE housing part.

vi) Drain valves to be opened, heated water to be discharged

vii) PHE used for the heating to be removed. Desired PHE to be inserted to the PHE housing part.

viii) Recording the results.

3.2.3.2. Operating Conditions and Test Setup

Number of EUT : 9 (9 EUTs 0.5 mm AISI 304L Top and Bottom Plates)

Medium : Water

CH Inlet Temperature : 72 ˚C

CH Outlet Temperature : 51 ˚C

DCW Inlet Temperature : 10 ˚C

DHW Outlet Temperature : 60 ˚C

CH Pressure : 1.5 bar

DHW Pressure : 10 bar

Assembly Position : EUTs assembled in housing to prevent any leakage at high pressures.

3.2.3.3. Functional Test Equipment Schematic

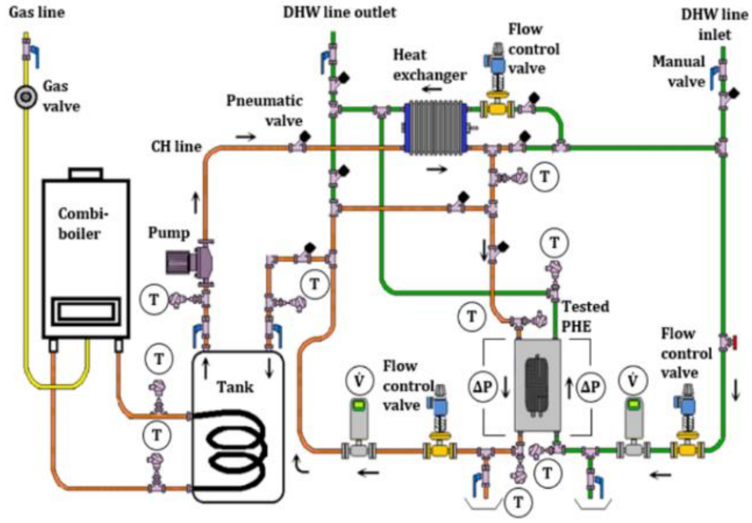

Figure 3.4. Functional Test Equipment Schematic (Kuzucanlı 2022)

3.2.3.4. Functional Test Equipment

Figure 3.5. Functional Test Kit

3.2.4. Theoretical Calculations for Functional Test

The equation used for calculation of heat output, effectiveness and heat capacity is:

$$Q_{DHW} = m_{DHW} C_p \Delta T \quad (38)$$

$$\varepsilon_{DHW} = \frac{Q_{DHW}}{Q_{max}} \quad (39)$$

$$\varepsilon_{CH} = \frac{Q_{CH}}{Q_{max}} \quad (40)$$

$$Q_{max} = C_{min}(T_{Ch,in} - T_{DCW}) \quad (41)$$

$$C_{min} = C_{DHW} = m_{DHW} c_p, \; m_{DHW} < m_{CH} \quad (42)$$

Q : Heat output, kW

Q_{max} : Maximum possible heat transfer rate, kW

ε : Effectiveness

C : Heat Capacity, kJ/̊C

c_p : Specific Heat Capacity, kJ/kg˚C

Table 3.3. Theoretical Calculations for 26 Plate AISI 304L Top Plate Used PHE

Theoretical Calculations for 26 Plate AISI 304L Top Plate Used PHE							
		Reference			Calculated Results		
Description	Unit	Average	Min	Max	Sample 1	Sample 2	Sample 3
DHW Heat Output	kW	35.2	35.1	35.3	35.2	35.3	35.1
DHW Effectiveness	-	0.308	0.306	0.311	0.308	0.311	0.306
CH Heat Output	kW	≥35			36.0	36.0	36.1
CH Effectiveness	-	0.327	0.326	0.329	0.328	0.326	0.329

Table 3.4. Theoretical Calculations for 24 Plate AISI 304L Top Plate Used PHE

Theoretical Calculations for 24 Plate AISI 304L Top Plate Used PHE							
		Reference			Calculated Results		
Description	Unit	Average	Min	Max	Sample 1	Sample 2	Sample 3
DHW Heat Output	kW	30.0	29.8	30.2	30.2	30.0	29.8
DHW Effectiveness	-	0.315	0.311	0.320	0.320	0.315	0.311
CH Heat Output	kW	≥30			30.9	30.7	30.7
CH Effectiveness	-	0.336	0.333	0.339	0.339	0.334	0.333

Table 3.5. Theoretical Calculations for 20 Plate AISI 304L Top Plate Used PHE

Theoretical Calculations for 20 Plate AISI 304L Top Plate Used PHE							
		Reference			Calculated Results		
Description	Unit	Average	Min	Max	Sample 1	Sample 2	Sample 3
DHW Heat Output	kW	24.2	24.1	24.3	24.1	24.2	24.3
DHW Effectiveness	-	0.321	0.318	0.324	0.318	0.321	0.324
CH Heat Output	kW	≥24			24.5	24.5	24.8
CH Effectiveness	-	0.336	0.332	0.342	0.332	0.334	0.332

Table 3.6. Theoretical Calculations for 26 Plate AISI 316L Top Plate Used PHE

Theoretical Calculations for 26 Plate AISI 316L Top Plate Used PHE							
		Reference			Calculated Results		
Description	Unit	Average	Min	Max	Sample 1	Sample 2	Sample 3
DHW Heat Output	kW	35.3	35.3	35.4	35.3	35.4	35.3
DHW Effectiveness	%	0.326	0.326	0.327	0.326	0.327	0.326
CH Heat Output	kW	36.0	35.7	36.3	35.7	36.3	36.0
CH Effectiveness	%	0.333	0.330	0.337	0.330	0.337	0.332

The findings of the test are presented in two sections: theoretical calculations and functional performance. Calculated heat production and observed DHW temperatures necessary to achieve acceptance requirements are included in the findings of thermal performance. Additional information is provided in the form of theoretical calculations, such as efficiency and DHW heat output.

3.2.5. FEA Analysis

Finite Element Method analysis has been conducted to simulate the burst effect, validate the findings for failure detection, and estimate deformation. The CAD model utilized comprises of flow channels, top and bottom plates, as well as internal plates. The analysis was simulated using a total of 32 cores. The time and resource utilization for the solution are presented below.

Table 3.7. Solution Time & Resource Usage

Status	Done
MAPDL Elapsed Time	19 h 56 m
MAPDL Memory Used	25.825 GB
MAPDL Result File Size	28.81 GB

The ANSYS Mechanical/Transient Structural Module was utilized to assess the surface deformation resulting from normal stress. The term "flexible dynamic analysis" is often used interchangeably with "transient structural analysis." This method can be employed to determine the dynamic behavior of a structure when subjected to arbitrary time-varying loads. The flexible dynamic analysis is a highly versatile technique that can be employed to ascertain the time-varying displacements, strains, stresses, and forces in a structure as it responds to transient loads.

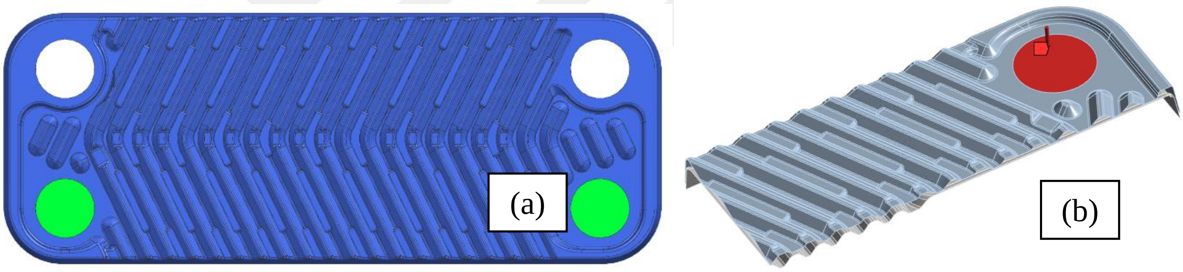

Figure 3.6. End Plate (a) / Load Impact Surface (b)

3.2.5.1. Boundary Conditions

In the numerical model, brazed regions are assumed as permanent connections. For this reason, bonded contact was defined in numerical models for the regions observed as brazed in the PHE samples. All other contact areas except brazed areas are modeled with frictional contact definition with a friction coefficient of 0.195.

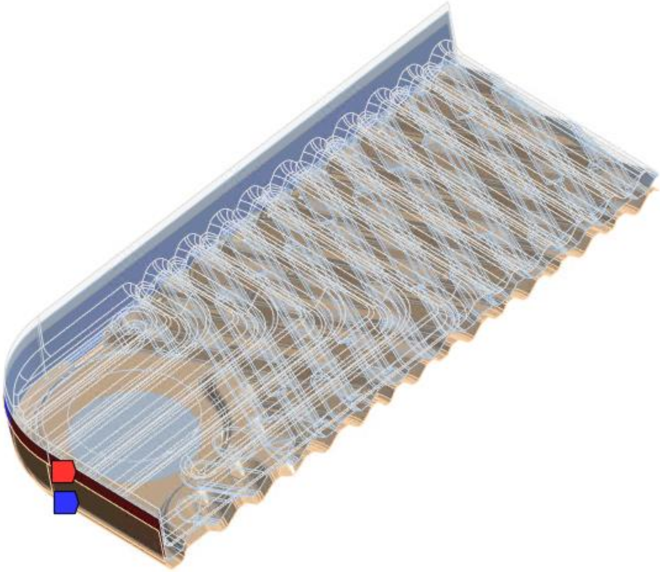

Figure 3.7. C-PHE Contact Surfaces

Choosing the appropriate contact type depending on the type of problem you are trying to solve is often tricky. Particularly, several new ANSYS users are very confused about the differences among the contact types, such as frictionless, rough, frictional, no separation. The bonded contact type is the prevailing configuration and is universally applied to all contact regions, including surfaces, solids, lines, faces, and edges. When contact regions are bonded, any movement involving sliding or separation between faces or edges is prohibited. Consider the region as being adhered together. This mode of contact facilitates a linear resolution as the length or area of contact remains constant throughout the load application. If contact is established based on the mathematical framework, any voids will be eliminated, and any initial intrusion will be disregarded.

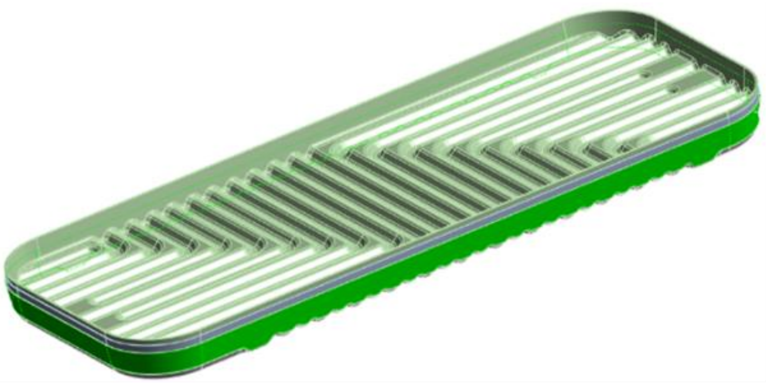

Figure 3.8. Top and Inner Plate of PHE

Symmetric quarter model method has been used to reduce FEA runtime since the effect and loads being applied to the component was symmetric. This technique is applicable solely to the surfaces of a given structure, without requiring any additional input from the user. When a symmetry plane condition is imposed on a face, the displacement of said face is constrained in the normal direction while remaining unrestricted in the tangential directions.

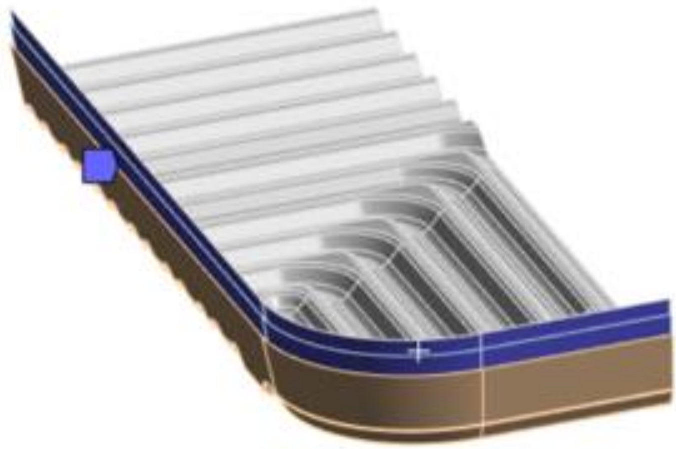

Figure 3.9. Sim Quarter Model Used For C-PHE

3.2.5.2. Load Profile

During the process of load distribution in the simulation setting, it is postulated that the dispersion of water towards the side plates beyond the inlet point is negligible. Additionally, it is assumed that the water attains a pressure of 36 bar at the highest point of the inner plate while preserving the pressure at the inlet point.

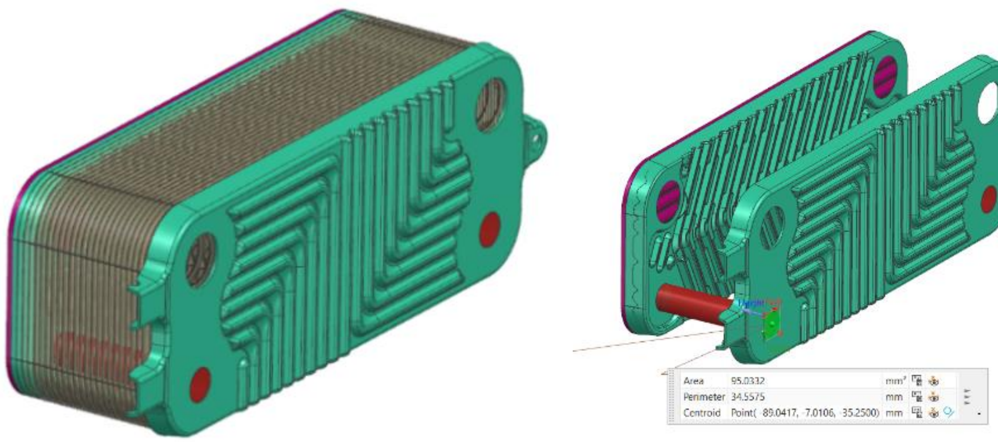

Figure 3.10. Compact Plate Heat Exchanger

The effect of 36 bar pressure on the end plate is reflected on the top plate. To demonstrate this in the simulation environment, the above-mentioned connection between the plates was defined and a pressure load of 36 bar was applied to the relevant surface on the end plate.

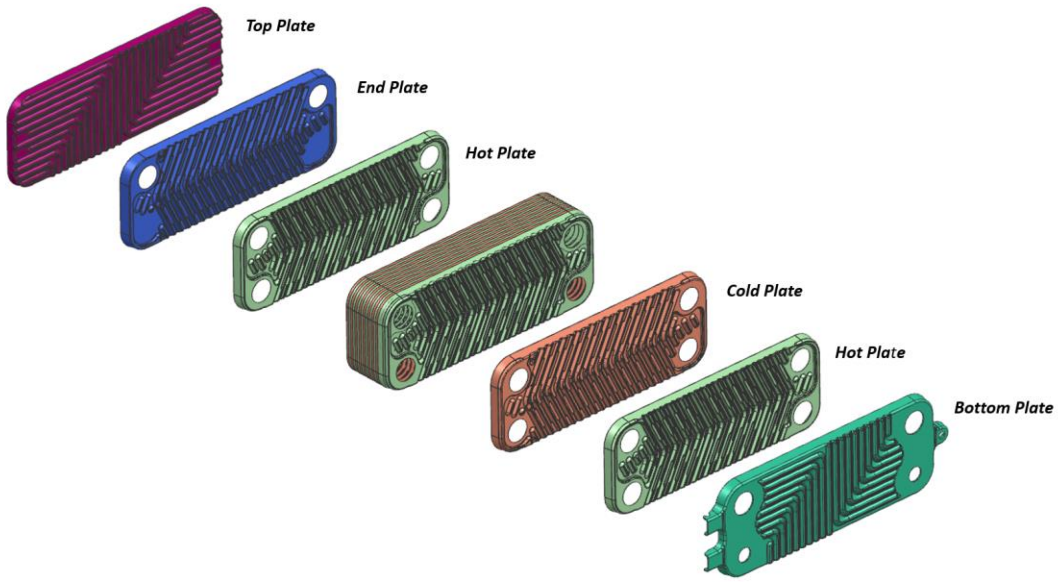

Figure 3.11. Plate Heat Exchanger Exploded View

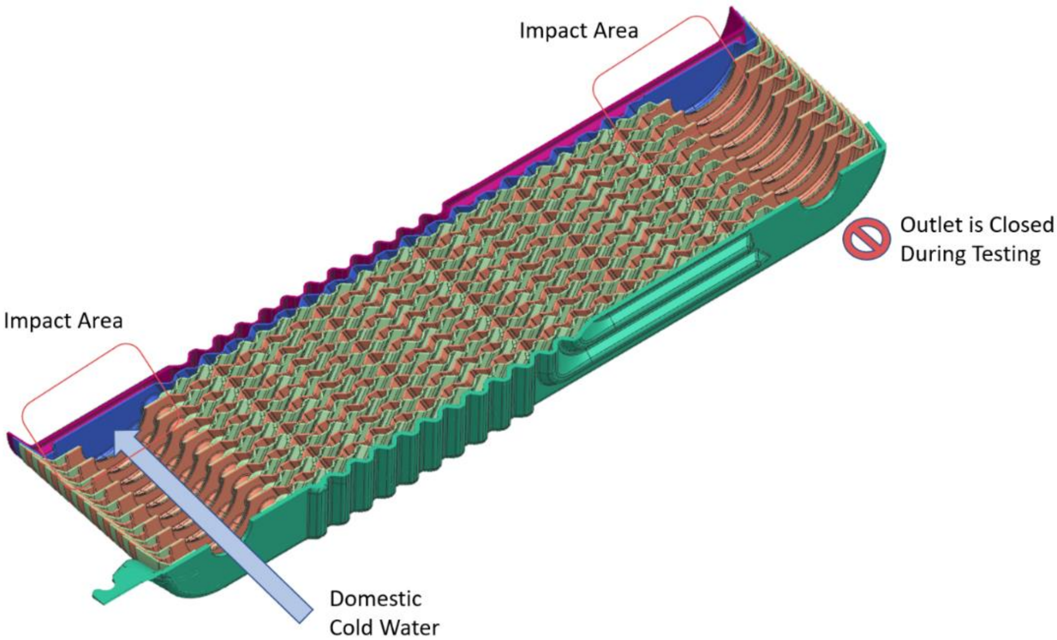

Figure 3.12. Demonstration of Impact Area

The DHW Output has been configured to be in a closed state, as per the experimental methodology. With this configuration it is guaranteed that the corresponding surface area will experience significant expansion.

The simulation method neglects the possibility of explosions at brazing points, and instead focuses on analyzing the deformation in the end and top plate. Pressure load profile used for the simulation is in the exact conditions which is applied in experimental method. The test description presented in Table 4 was:

- Raise pressure to 6 bar wait and observe for 180 seconds.
- Raise pressure to 12 bar wait and observe for 180 seconds.
- Raise pressure to 18 bar wait and observe for 180 seconds.
- Raise pressure to 24 bar wait and observe for 180 seconds

(Deformation starts according to burst performance test results).

- Raise pressure to 30 bar wait and observe for 180 seconds.
- Raise pressure to 36 bar wait and observe for 180 seconds.

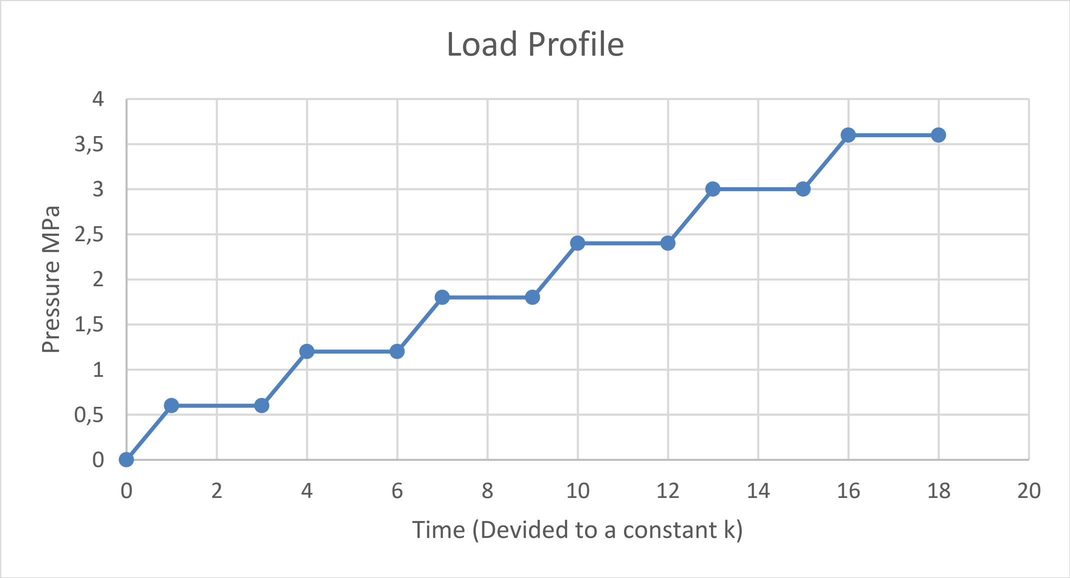

Figure 3.13. Burst Test Pressure Load Profile

3.2.5.3. Meshing

For meshing, elements with average size of 0.33 mm were used. Number of nodes have been used is 177110. Number of elements is 171081. Higher density of the elements was used for blend corners which can been seen in the Figure 27. And finally, 2D quad and triangle were used for complete meshing.

Figure 3.14. Mesh Modelling

3.2.5.4. Material Database

Multilinear Isotropic Hardening material model was used for modelling of AISI 316L Steel. Relevant material properties have been taken from Ansys Granta Material Database.

Table 3.8. Material Properties of AISI 316L

Property	Value	Unit
Density	7969.4	kgm^{-3}
Derive from	Young’s Modulus and Poisson’s Ratio	
Young’s modulus	1.9736x10^{5}	MPa
Poisson’s Ratio	0.26995	
Bulk Modulus	1.4298x10^{11}	Pa
Shear Modulus	7.7703x10^{10}	Pa
Active Table	Total	
Yield Strength	229.57	MPa
Tangent Modulus	1240	MPa
Isotropic Thermal Conductivity	14.886	$Wm^{-1}C^{-1}$
Specific Heat Constant Pressure	509.61	$Jkg^{-1}C^{-1}$
Isotropic Resistivity	7.476x10^{7}	Ohm m

The characterization of material properties is a crucial initial step in the representation of any material model within the context of FEA. Incorrect input of material details can significantly impact the outcome. If erroneous data is fed into the FEA system, the resulting output will inevitably be inaccurate. It is imperative to be mindful of the material details that are being inputted into FEA.

The process of defining a material in FEA is comparatively less intricate than the task of accurately representing the physical properties of the material. Diverse material specifications, including but not limited to yield stress, ultimate stress, young modulus, Poisson ratio, bulk modulus, thermal conductivity, elongation, specific heat, stress vs strain curve, and electric properties, are inherent to tangible materials. In the context of FEA, it is not necessary to specify all material details to model the material. The specific material details required are contingent upon the type of FE analysis being conducted, such as linear or nonlinear solutions, static or dynamic analyses, and steady state or time-dependent analyses, among others. The tabulated data denotes the essential material characteristics that are mandated for fundamental finite element analysis categories.

Table 3.9. Materials as per FE Analysis (Graspengineering, 2022)

Material Properties	Linear Static	Non-Linear Contact	Non-Linear Material	Non-Linear Dynamic	Fatigue	(Linear Dynamics) Modal, Seismic Frequency Response	Thermal	Thermal Structural	Transient Structural
Young's Modulus	Yes	Yes	Yes	Yes	Yes	Yes		Yes	Yes
Mass Density	Yes	Yes	Yes	Yes	Yes	Yes		Yes	Yes
Thermal Conductivity	Yes	Yes	Yes	Yes	Yes	Yes		Yes	Yes
Thermal Expansion							Yes		
Specific Heat								Yes	
Stress-Strain Curve			Yes						Yes
Fatigue Life Curve (SN Curve					Yes				

The analysis of transients may be thermal or structural. By definition, a transient analysis includes loads that depend on time. A structure's dynamic reaction to any form of general time-dependent stress is evaluated using a transient type of study. In experiment method load time was a crucial factor so that this type of method is selected for the FEA analysis.

4. RESULTS

4.1. Mechanical Strength Performance Result of AISI 304L 0.5 mm Top Plate Used PHE

The material was chosen as AISI 304L and AISI 316L by comparing the availability status from the suppliers with the properties of forming, welding, and resisting corrosion. These materials, which are actively used by most plate heat exchanger manufacturers, have been subjected to price evaluation. AISI 304L material is cheaper because it contains less nickel. Nickel has the property of increasing the expansion forming ability. At the same time, the idea of reducing the thickness of the material, which is another cost reductive method, was evaluated.

The reason for material changes on the only top plate is, to keep the material associated with the heat transfer the same and to preserve the output values of the heat exchanger. After the selected material has been processed, the production of plate heat exchangers has been completed and has been subjected to performance evaluation tests.

Burst test was performed to determine the maximum pressure value that the plate heat exchanger can withstand without deformation and results were obtained. These results revealed that deformation was observed on the top plate of the sample at a certain pressure which is 16 bar for 0.5 mm AISI 304L top plated PHE and 24 bar for 0.5 mm AISI 316L top plated PHE. Deformation measurement analysis has been performed in two different methods. Probe measurement on top plate of the deformed product and cut-out scanning of relevant cross-sectional surface.

Table 4.1. Sample Information

Sample Name	**Test Pressure (bar)**
S2 26 Plate AISI 304L Top Plate Used PHE	36
T1 26 Plate AISI 316L Top Plate Used PHE	36

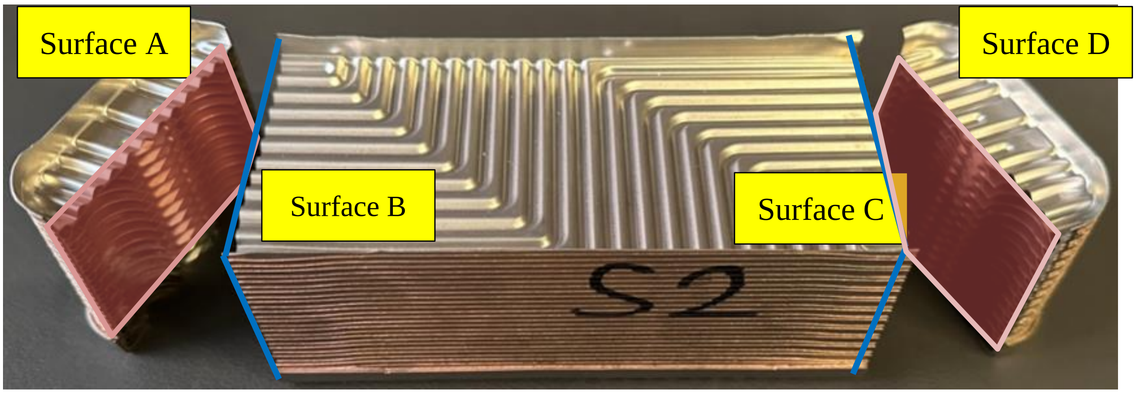

Figure 4.1. AISI 304L Top Plate 36 bar Used Sample

The plate heat exchanger sample that was cut following deformation and the corresponding surface designations are shown in Figure 28. The channels were measured in samples obtained from the cross section to thoroughly analyze the impact of the degradation in the inner channels after the application of loads. The difference between the ideal condition and the ideal condition was then assessed using the cad data. Measured max deformation can be found with the calculation of average value of the eleven internal channel height and measured value of deformed channel by ImageJ. Deformation values is the difference between those two values.

4.1.1. 0.5 mm AISI 304L Top Plate Used PHE Sample 1 (36 bar Max) Cross Section Surface A Measurement Results

Figure 4.2. ImageJ Channel Port Measurement for AISI 304L Top Plate Used PHE Sample Surface A (36 bar Max)

Table 4.2. Channel Port Dimension Check for 0.5 mm AISI 304L Top Plate Used PHE Sample 1 Surface A (36 bar Max)

	Channel Height (mm)
1	3.312
2	3.362
3	3.319
4	3.323
5	3.305
6	3.337
7	3.284
8	3.326
9	3.337
10	3.358
11	3.358

Table 4.3. Channel Port Dimension Deviation for 0.5 mm AISI 304L Top Plate Used PHE Sample 1 Surface A (36 bar Max)

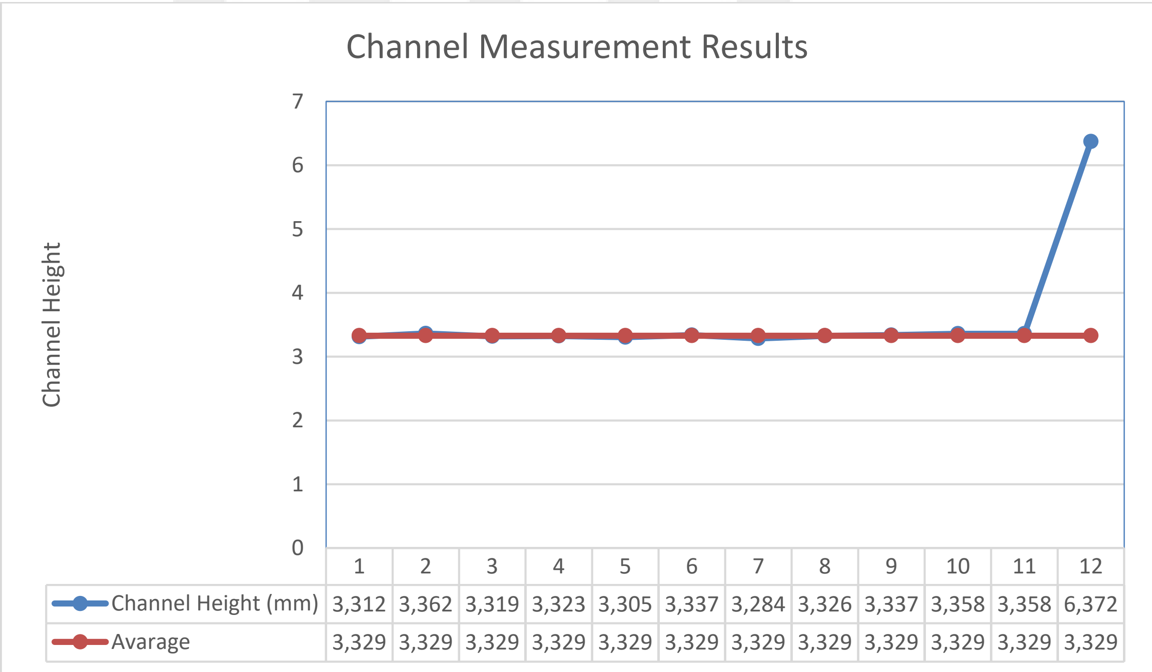

Even though the channel size was initially set to 3.5mm in the CAD software for the inner plates, the data presented in the Table 4.3 indicates that there has been a deviation from this value. The rationale behind this practice is that a certain amount of force is exerted on the component during its manufacturing process, and it is subsequently maintained under that load. The process mentioned earlier is of utmost importance in facilitating the creation of points of contact among the plates. Insufficient weight placement to maintain the duct size can result in weakened connection points, commonly referred to as brazing points, between the ducts.

This, in turn, can lead to internal leakage in the final product. The phenomenon of internal leakage occurs when there is a mixing of CH and DCW water, resulting in the domestic water exceeding the prescribed limits set by global standards. This occurrence is particularly concerning as it leads to a loss of pressure within the component. Consequently, the product is unable to perform its intended purpose. The results of the functional tests conducted on the heat exchanger, which included the inner plate channels with dimensions specified in Table 4.3, did not indicate any loss of value.

Table 4.4. Measured Maximum Deformation for 0.5 mm AISI 304L Top Plate Used PHE Sample 1 Surface A (36 bar Max)

Standard Deviation	0.023
Average	3.329
12 Deformed Channel Height (mm)	6.372
Measured Max Deformation (mm)	3.042

The height measurements of the initial 11 channels were averaged in the conducted measurements. The dimensions of the 12th channel were determined through the utilization of scaling and measurement methodology employing ImageJ software. By utilizing this parameter, the disparity in mean channel length was mitigated through subtraction, and the magnitude of distortion in the corresponding channel altitude was computed.

4.1.2. 0.5 mm AISI 304L Top Plate Used PHE Sample 1 (36 bar Max) Cross Section Surface B Measurement Results

Figure 4.3. ImageJ Channel Port Measurement for AISI 304L Top Plate Used PHE Sample Surface B (36 bar Max)

Measurements were conducted on surface b, which constitutes the opposite side of surface a within the identical cross-sectional area. The objective of this is to demonstrate that the deformation transpires not at a solitary point but rather by disseminating superficially on the surface where the water under pressure makes contact. The study utilized a cross-sectional sample and conducted a scan to investigate the inter-channel situation.

Table 4.5. Channel Port Dimension Check for 0.5 mm AISI 304L Top Plate Used PHE Sample 1 Surface B (36 bar Max)

	Channel Height (mm)
1	3.282
2	3.388
3	3.261
4	3.261
5	3.282
6	3.303
7	3.24
8	3.303
9	3.324
10	3.303
11	3.346

Table 4.6. Channel Port Dimension Deviation for 0.5 mm AISI 304L Top Plate Used PHE Sample 1 Surface B (36 bar Max)

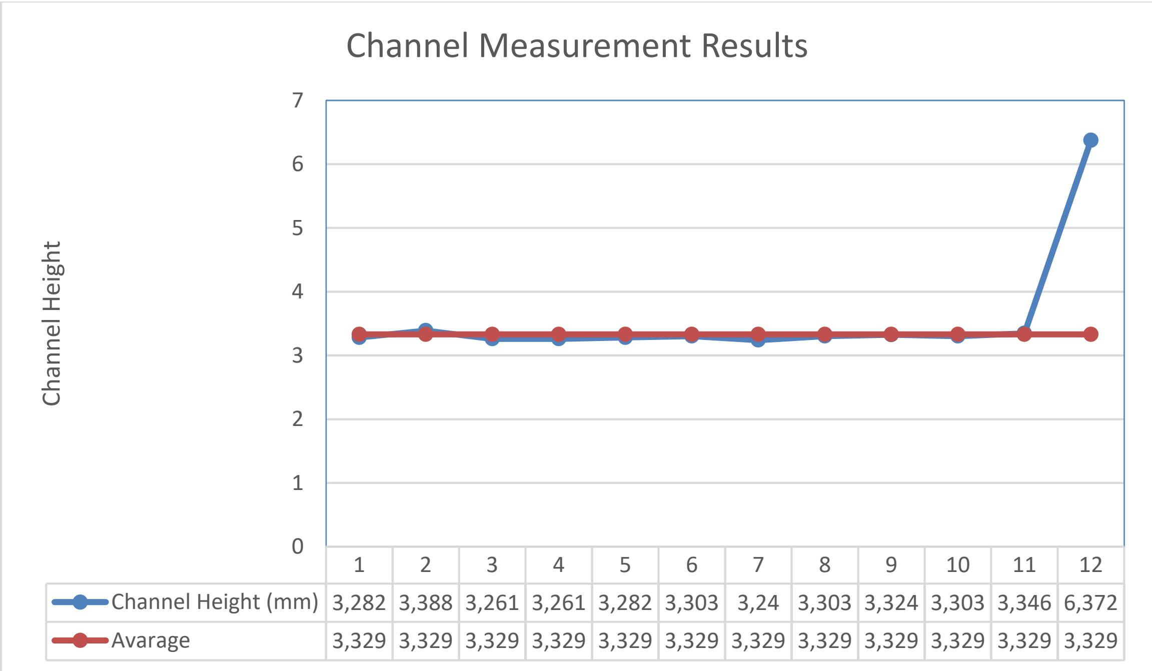

The heights of the channels created by the internal plates were quantified, and subsequently, the mean channel height observed in the cross-section of this surface was determined along with the corresponding standard deviation.

Table 4.7. Measured Maximum Deformation for 0.5 mm AISI 304L Top Plate Used PHE Sample 1 Surface B (36 bar Max)

Standard Deviation	0.040
Average	3.299
12 Deformed Channel Height (mm)	6.422
Measured Max Deformation (mm)	3.122

Following the determination of the standard deviation and mean value, the measurement of the 12th channel size was conducted utilizing ImageJ. The dissimilarity between the computed mean channel magnitude and the observed size of the 12th channel is adequate to derive the deformation parameter

4.1.3. 0.5 mm AISI 304L Top Plate Used PHE Sample 1 (36 bar Max) Cross Section Surface C Measurement Results

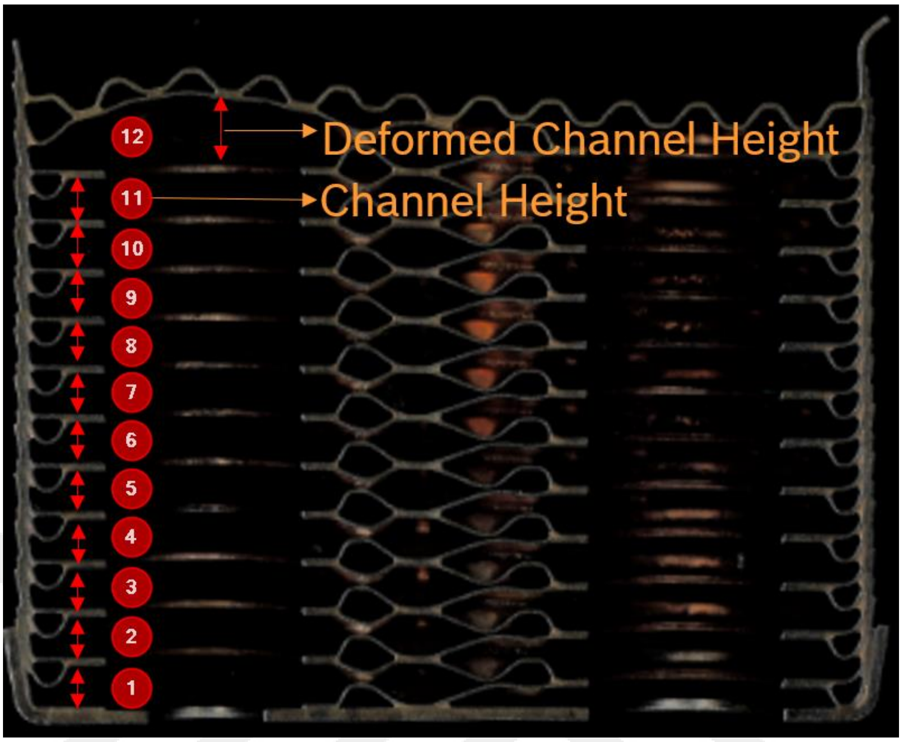

Figure 4.4. ImageJ Channel Port Measurement for AISI 304L Top Plate Used PHE Sample 1 Surface C (36 bar Max)

Channel dimensions in surface C showed in Figure 4.4 has been measured with same method and documented as below.

Table 4.8. Channel Port Dimension Check for 0.5 mm AISI 304L Top Plate Used PHE Sample 1 Surface C (36 bar Max)

	Channel Height (mm)
1	3.411
2	3.305
3	3.263
4	3.312
5	3.305
6	3.305
7	3.305
8	3.39
9	3.347
10	3.305
11	3.39

Table 4.9. Channel Port Dimension Deviation for 0.5 mm AISI 304L Top Plate Used PHE Sample 1 Surface C (36 bar Max)

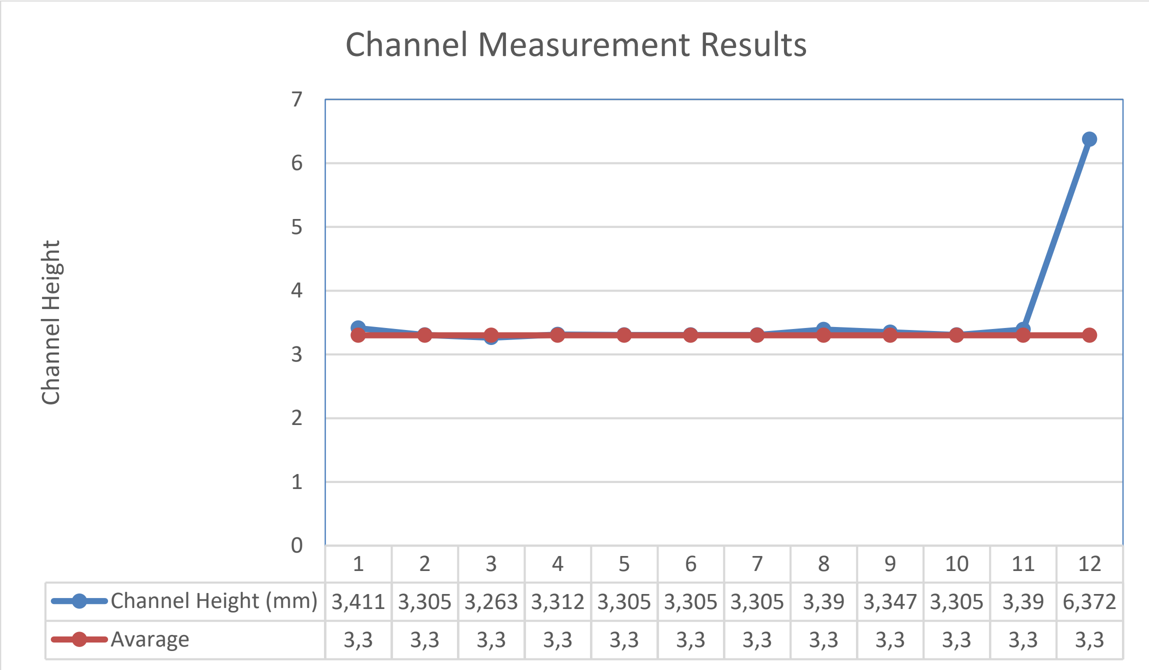

The measurements specified in Table 4.8 are quite close to the measurement results in Table 4.6 and 4.4. Based on this deduction, it can be inferred that the structure of plate heat exchanger channels under pressure does not vary significantly at the points where pressurized water enters and exits, and that the changes in the channel structure are similar.

Table 4.10. Measured Maximum Deformation for 0.5 mm AISI 304L Top Plate Used PHE Sample 1 Surface C (36 bar Max)

Standard Deviation	0.044
Average	3.330
12 Deformed Channel Height (mm)	6.063
Measured Max Deformation (mm)	2.732

The 12th channel height measurement was obtained as 6.063 through the utilization of ImageJ software. The mean channel height observed in the specimen was 3.330 mm. The difference between these quantities indicates the deformation of the end plate, which is being shared with the upper plate. The value for surface C can be determined as 2.732mm.

It is expected that the direct contact points on the input and output surfaces of the upper plate will be deformed in similar proportions due to the closed exit valve condition during the experimental setup. Currently, there exists a significant disparity between the deformation values at the points where pressurized water enters and exits. At the point of entry of the water, a higher deformation value was observed, whereas there was almost no deformation observed at the interface near the exit point. The impact of this can be identified as sudden loading during pressurization in the experimental procedure. When water under high pressure enters the plate heat exchanger, it creates a significant deformation on the surface it first contacts, which results in an unclear interpretation of the designed analysis. Therefore, the pressure application device utilized during the experiment was substituted with an electronic pressure application device that can present a more linear distribution of load.

4.1.4. 0.5 mm AISI 304L Top Plate Used PHE Sample 1 (36 bar Max) Cross Section Surface D Measurement Results

Figure 4.5. ImageJ Channel Port Measurement for AISI 304L Top Plate Used PHE Sample 1 Surface D (36 bar Max)

The dimensions of the channel extracted from the surface scan indicated as D in Figure 4.1 were measured using the same methodology and recorded as follows:

Table 4.11. Channel Port Dimension Check for 0.5 mm AISI 304L Top Plate Used PHE Sample 1 Surface D (36 bar Max)

	Channel Height (mm)
1	3.284
2	3.284
3	3.305
4	3.263
5	3.298
6	3.326
7	3.284
8	3.284
9	3.326
10	3.326
11	3.326

Table 4.12. Channel Port Dimension Deviation for 0.5 mm AISI 304L Top Plate Used PHE Sample 1 Surface D (36 bar Max)

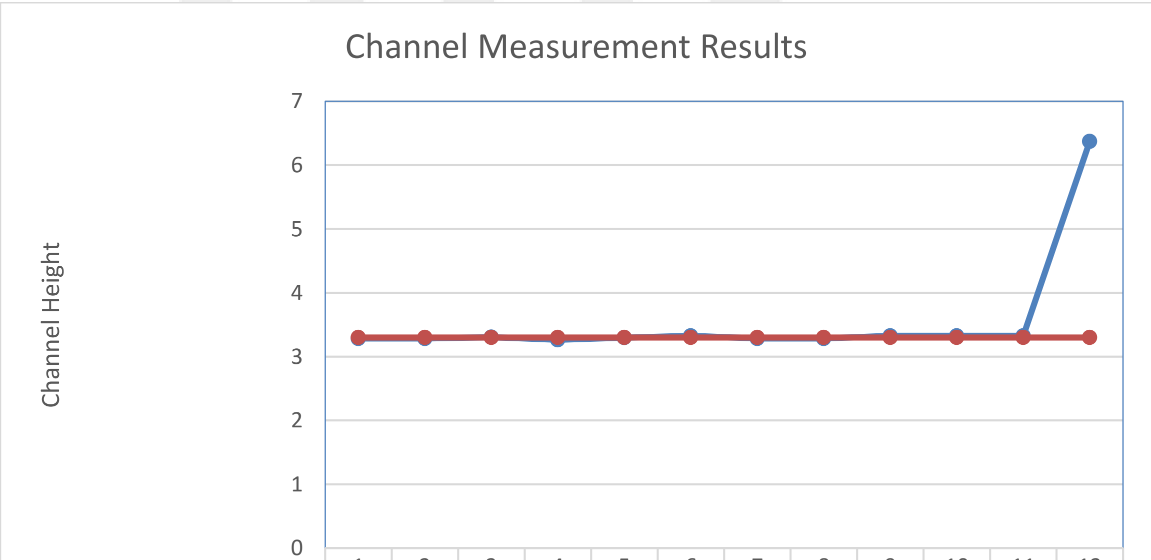

	1	2	3	4	5	6	7	8	9	10	11	12
Channel Height (mm)	3,284	3,284	3,305	3,263	3,298	3,326	3,284	3,284	3,326	3,326	3,326	6,372
Avarage	3,3	3,3	3,3	3,3	3,3	3,3	3,3	3,3	3,3	3,3	3,3	3,3

The measurements defined in 19 show a considerable proximity to the measurement outcomes presented in Table 17-15-13. Based on this deduction, it can be inferred that the structure of plate heat exchanger channels under pressure does not vary significantly at the points where pressurized water enters and exits, and that the changes in the channel structure are similar.

Table 4.13. Measured Maximum Deformation for 0.5 mm AISI 304L Top Plate Used PHE Sample 1 Surface D (36 bar Max)

Standard Deviation	0.021
Average	3.300
12 Deformed Channel Height (mm)	5.994
Measured Max Deformation (mm)	2.693

The 12th measurement of channel height was acquired as 5.994 via the application of ImageJ software. The observed average channel height in the specimen was 3.300 mm. The disparity among these magnitudes denotes the distortion of the end plate, which is being distributed with the top plate. The deformation value on top plate from surface D can be ascertained to be 2.693 millimeters.

4.2. Mechanical Strength Performance Result of AISI 316L 0.5 mm Top Plate Used PHE

4.2.1. 0.5 mm AISI 316L Top Plate Used PHE Sample 1 (36 bar Max) Cross Section Surface A Measurement Results

The deformation of the plate heat exchanger, which was constructed with a top plate composed of AISI 316L material, was determined using an identical approach and technique. The deformation of the plate heat exchanger was expected to be lower in the AISI 316L type due to its varying nickel content. Similar procedures were implemented in the sample.

The specimen, which has undergone pressurization and deformation, is dispatched for precise incisions at designated positions corresponding to the water inlet sites. Received samples have been scanned and measurements completed by scaling method using ImageJ.

Figure 4.6. AISI 316L Top Plate Used C-PHE Cut-Out Sample

Figure 4.7. ImageJ Channel Port Measurement for AISI 316L Top Plate Used PHE Sample 1 Surface A (36 bar Max)

The results indicate that the heat exchanger fabricated with a AISI 316L top plate exhibited a lower degree of deformation, despite being subjected to identical loads and profile as AISI 304L used plate heat exchanger.

Table 4.14. Channel Port Dimension Check for 0.5 mm AISI 316L Top Plate Used PHE Sample 1 Surface A (36 bar Max)

	Channel Height (mm)
1	3.164
2	3.347
3	3.305
4	3.319
5	3.369
6	3.347
7	3.305
8	3.347
9	2.637
10	3.369
11	3.39

The measurements defined in Table 4.14 exhibit a high degree of proximity to the measurement outcomes presented in AISI 304L used sample. Since internal plate materials and applied pressures are the same there is no significant difference between internal channel heights.

Table 4.15. Channel Port Dimension Deviation for 0.5 mm AISI 316L Top Plate Used PHE Sample 1 Surface A (36 bar Max)

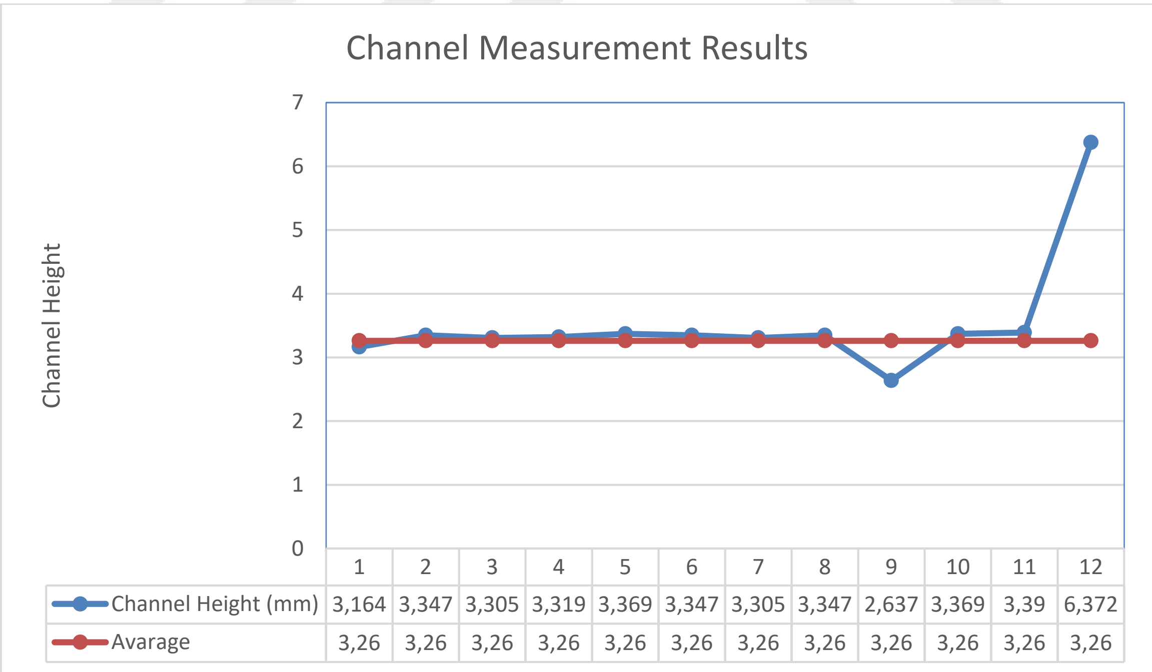

The measurements defined in Table 21 exhibit a high degree of proximity to the measurement outcomes presented in AISI 304L used sample. Since internal plate materials and applied pressures are the same there is no significant difference between internal channel heights.

Table 4.16. Measured Maximum Deformation for 0.5 mm 316L Top Plate Used PHE Sample 1 Surface A (36 bar Max)

Standard Deviation	0.206
Average	3.263
12 Deformed Channel Height (mm)	4.26
Measured Max Deformation (mm)	0.996

The 12th channel height measurement was obtained as 4.26 through the utilization of ImageJ software. The mean channel height observed in the specimen was 3.26 mm. The difference between these quantities indicates the deformation of the end plate, which is being shared with the upper plate. The value for surface A can be determined as 0.996 mm.

4.2.2. 0.5 mm AISI 316L Top Plate Used PHE Sample 1 (36 bar Max) Cross Section Surface B Measurement Results

Figure 4.8. ImageJ Channel Port Measurement for AISI 316L Top Plate Used PHE Sample 1 Surface B (36 bar Max)

As depicted in Figure 4.8, The measurement of the other side of the taken specimen is important in terms of examining the point distribution of deformation. Therefore, an evaluation and interpretation of the distances on this surface have been conducted.

Table 4.17. Channel Port Dimension Check for 0.5 mm AISI 316L Top Plate Used PHE Sample 1 Surface B (36 bar Max)

	Channel Height (mm)
1	3.241
2	3.404
3	3.39
4	3.347
5	3.39
6	3.319
7	3.411
8	3.368
9	3.347
10	3.39
11	3.368

Table 4.18. Channel Port Dimension Deviation for 0.5 mm AISI 316L Top Plate Used PHE Sample 1 Surface B (36 bar Max)

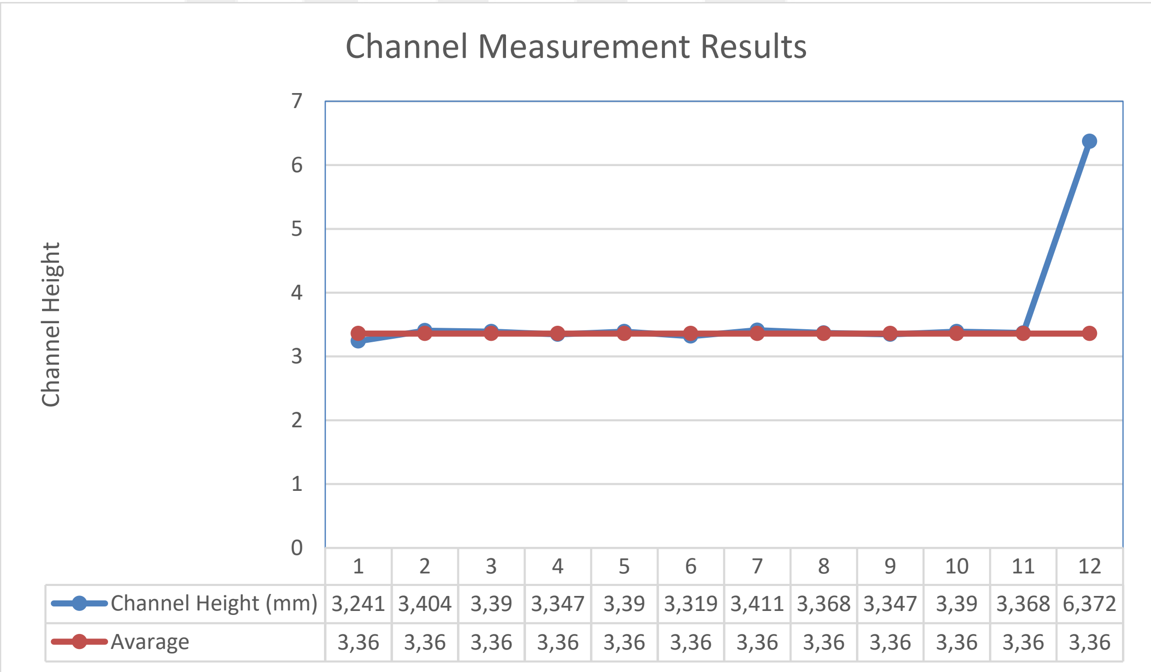

Table 4.18 displays minor variations observed between the two sides of the section. This phenomenon occurs due to the distribution of surface deformation in a linear manner across the top plate surface following the application of pressure. The finite element method will be utilized in subsequent stages to conduct an analysis of these minor discrepancies.

Table 4.19. Measured Maximum Deformation for 0.5 mm 316L Top Plate Used PHE Sample 1 Surface B (36 bar Max)

Standard Deviation	0.046
Average	3.360
12 Deformed Channel Height (mm)	4.11
Measured Max Deformation (mm)	0.748

The 12th measurement of channel height was acquired as 4.11 via the application of ImageJ software. The observed average channel height in the specimen was 3.36 mm. The disparity among these magnitudes denotes the distortion of the end plate, which is being distributed with the top plate. The deformation value on top plate from surface D can be ascertained to be 0.748 millimeters.

4.2.3. 0.5 mm AISI 316L Top Plate Used PHE Sample 1 (36 bar Max) Cross Section Surface C Measurement Results

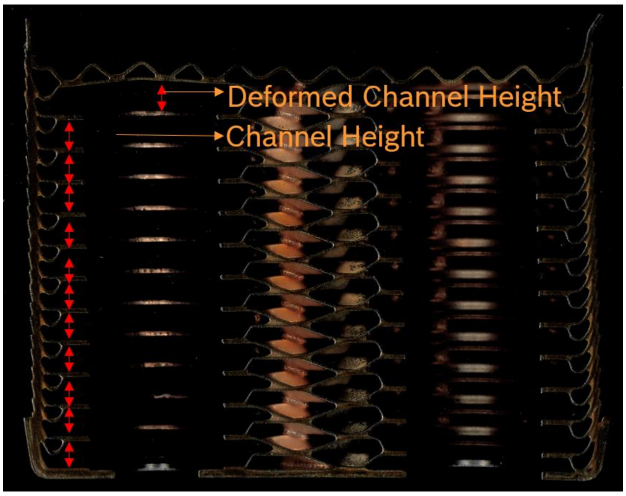

Figure 4.9. ImageJ Channel Port Measurement for AISI 316L Top Plate Used PHE Sample 1 Surface C (36 bar Max)

Channel dimensions in Figure 4.9 has been measured with same method and documented as below.

Table 4.20. Channel Port Dimension Check for 0.5 mm AISI 316L Top Plate Used PHE Sample 1 Surface C (36 bar Max)

	Channel Height (mm)
1	3.47
2	3.512
3	3.45
4	3.47
5	3.514
6	3.492
7	3.512
8	3.493
9	3.512
10	3.469
11	3.534

Table 4.21. Measured Maximum Deformation for 0.5 mm 316L Top Plate Used PHE Sample 1 Surface C (36 bar Max)

Standard Deviation	0.02465531
Average	3.493454545
12 Deformed Channel Height (mm)	4.58
Measured Max Deformation (mm)	1.086

Table 4.22. Channel Port Dimension Deviation for 0.5 mm AISI 316L Top Plate Used PHE Sample 1 Surface C (36 bar Max)

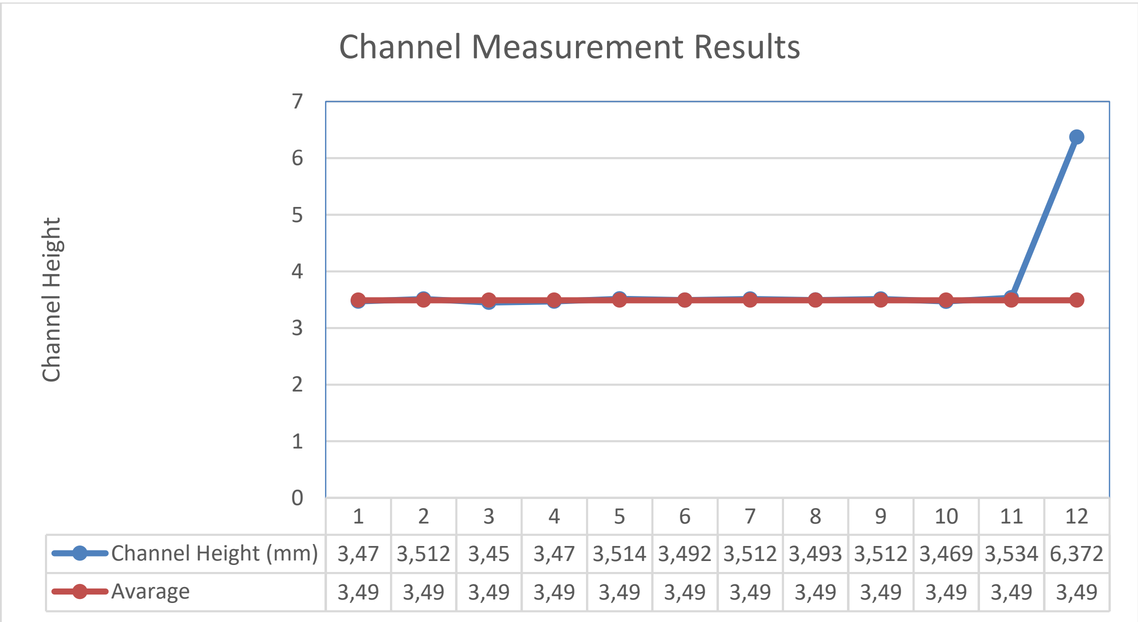

The 12th channel height measurement was obtained as 4.58 through the utilization of ImageJ software. The mean channel height observed in the specimen was 3.49 mm. The difference between these quantities indicates the deformation of the end plate, which is being shared with the upper plate. The value for surface C can be determined as 1.08 mm.

4.2.4. 0.5 mm AISI 316L Top Plate Used PHE Sample 1 (36 bar Max) Cross Section Surface D Measurement Results

Figure 4.10. ImageJ Channel Port Measurement for AISI 316L Top Plate Used PHE Sample 1 Surface D (36 bar Max)

Channel dimensions in Figure 4.10 has been measured with same method and documented as below.

Table 4.23. Channel Port Dimension Check for 0.5 mm AISI 316L Top Plate Used PHE Sample 1 Surface D (36 bar Max)

	Channel Height (mm)
1	3.291
2	3.462
3	3.419
4	3.397
5	3.433
6	3.462
7	3.397
8	3.44
9	3.492
10	3.433
11	3.504

Table 4.24. Channel Port Dimension Deviation for 0.5 mm AISI 316L Top Plate Used PHE Sample 1 Surface D (36 bar Max)

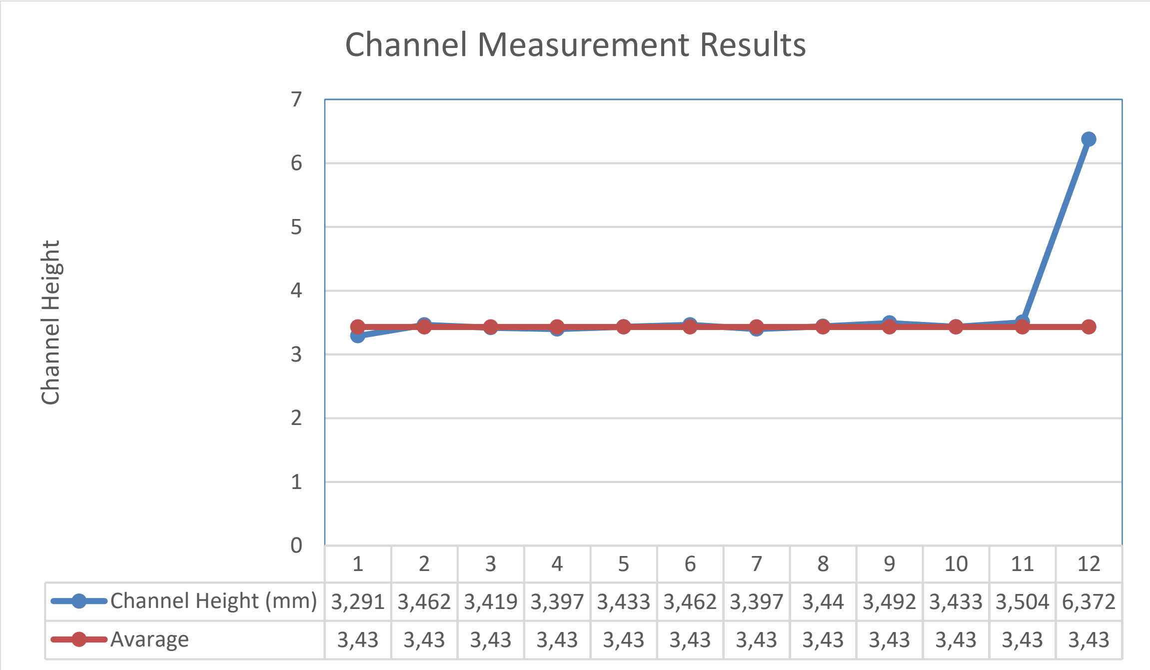

Table 4.25. Measured Maximum Deformation for 0.5 mm 316L Top Plate Used PHE Sample 1 Surface D (36 bar Max)

Standard Deviation	0.054
Average	3.43
12 Deformed Channel Height (mm)	4.48
Measured Max Deformation (mm)	1.05

The 12th measurement of channel height was acquired as 4.48 via the application of ImageJ software. The calculated average channel height in the specimen was 3.43 mm. The difference among these magnitudes denotes the distortion of the end plate, which is being distributed with the top plate. The deformation value on top plate from surface D can be ascertained to be 1.05 millimeters.

During the experiments, no deformation was observed at a pressure of 15 bar in the section that is in direct contact with the deformed surface. This situation demonstrates that the deformation occurring in 15 bar is due to sudden changes in pressure during application, and that more accurate results can be obtained through a controlled experimental setup. One way to demonstrate this is by producing new samples using the same material and subjecting them to retesting through the steps described in the procedure, but with the support of a different compression device.

At this stage, the procurement of AISI 304L material with a thickness of 0.5 mm and AISI 316L material with a thickness of 0.5 mm for the top plate were used to fulfill the required tests.

The produced samples were subjected to a compression test, and after reaching 24 bar for AISI 316L top plate used PHE and 18 bar for AISI 304L used PHE, deformations on the upper plate were observed quantitatively.

The distortions were measured using a Probe device to minimize the spring back effect that may occur after the cutting process and to present a different method within the thesis, resulting in a more accurate outcome.

4.3. Mechanical Strength Performance Result of AISI 316L & AISI 304L 0.5 mm Top Plate Used PHE

Manufactured components have been pressurized with more effective method with assist of electronic elements and precise air filter regulator. Maximator Burst Test apparatus can reflect even 0.1 bar increments on its screen. With the precise filling mechanism, it is possible to increase the pressure in decimal values.

Table 4.26. Pressure Load Application with Maximator Test Equipment

Pressure (bar)	Test Apparatus Load
0 6	**1st Load**
6 12	**2nd Load**
12 18	**3rd Load**
18 24	**4th Load**
24 30	**5th Load**
30 36	**6th Load**

The top plates of the deformed samples were measured with the probe by taking references from the specified points which has been given in Figure 38.

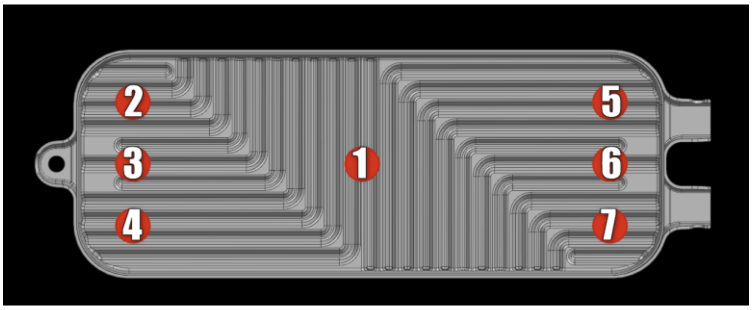

Figure 4.11. CAD Dimension Reference for Probe Measurement

The number one measurement point is in the center and is outside the influence of the domestic pressure field. For this reason, this point was taken as the zero point in the samples whose production was completed, and the deviation amounts were measured by calculating the delta between the other specified points and this point. Surface number 7 is the projection on the upper plate of the surface where the mains pressure enters the system directly. The 4th surface is the projection on the upper plate of the surface where the mains water comes out of the plate heat exchanger in a heated state. The measurement results to be taken at these points are the most critical for evaluation. Because these surfaces, which are in direct interaction with the high mains pressure, are in vertical contact with the water flow. The result of the force effect of the relevant pressure on the unit surface area multiplied by the pressure value with the surface area at the vertical contact point is interpreted.

Figure 4.12. Probe Measurement Device

Probe measuring device is a tool that allows measuring distances by taking point measurements at different reference points after a specified reference. The probe head and the planar elements it contains are very useful for the metric measurement of uneven surfaces, which are also found on the top plate of the plate heat exchanger. The amount of deformation occurred in the plate heat exchanger sample produced with AISI 316L 0.5 mm top plate and AISI 304L 1 mm top plate by this method was measured and listed.

It can be interpreted that sometimes a section on the upper plate has a negative slope. It should be noted that the reason for this may be the plates not sitting perfectly aligned with each other before the punching process during production, or due to various production parameters that cannot be controlled such as small angle difference before weight stacking process.

During the testing procedure, a probe measuring device was utilized to quantify the extent of deformation, an electronic pressurization element was employed to apply pressure, and fixing element materials were utilized to maintain the heat exchanger in a constant state. The prescribed methodology outlined in Table 4 was employed to pressurize the test components, while the deformation quantities at the designated locations as depicted in Figure 40 were recorded at six bar intervals. Thus, a significant correlation was established between the load applied and the deformation of the upper plate.

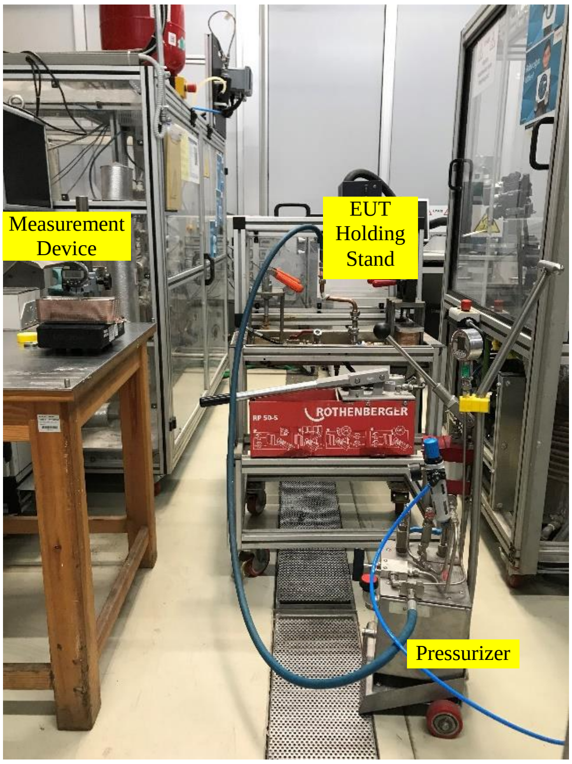

Figure 4.13. Test Stand for PHE Deformation

Table 4.27. Probe Measurement Results

		Measurement Results (mm)					
Material	Measurement Point	At 6 bar	At 12 bar	At 18 bar	At 24 bar	At 30 bar	At 36 bar
AISI 304L 0.5 mm Top Plate Used PHE	1 (Ref Point)	0	0	0	0	0	0
	2	-0.67	-0.55	-0.44	-0.37	-0.25	-0.12
	3	0.09	0.11	0.12	0.15	0.37	0.45
	4	0.46	0.57	0.59	1.02	1.79	2.54
	5	0.10	0.12	0.13	0.13	0.15	0.28
	6	0.11	0.13	0.13	0.15	0.21	0.28
	7	0.12	0.25	0.53	0.97	1.47	2.31
AISI 316L 0.5 mm Top Plate Used PHE	1 (Ref Point)	0	0	0	0	0	0
	2	0.28	0.28	0.29	0.29	0.35	0.42
	3	0.05	0.07	0.1	0.12	0.18	0.24
	4	0.28	0.32	0.40	0.51	0.73	1.25
	5	0.37	0.37	0.38	0.39	0.45	0.48
	6	0.25	0.27	0.29	0.32	0.39	0.43
	7	0.24	0.32	0.44	0.58	0.79	1.1

Table 4.28. Total Deformation on the Surface Measurement Points for 0.5 mm AISI 304L Top Plate Used PHE

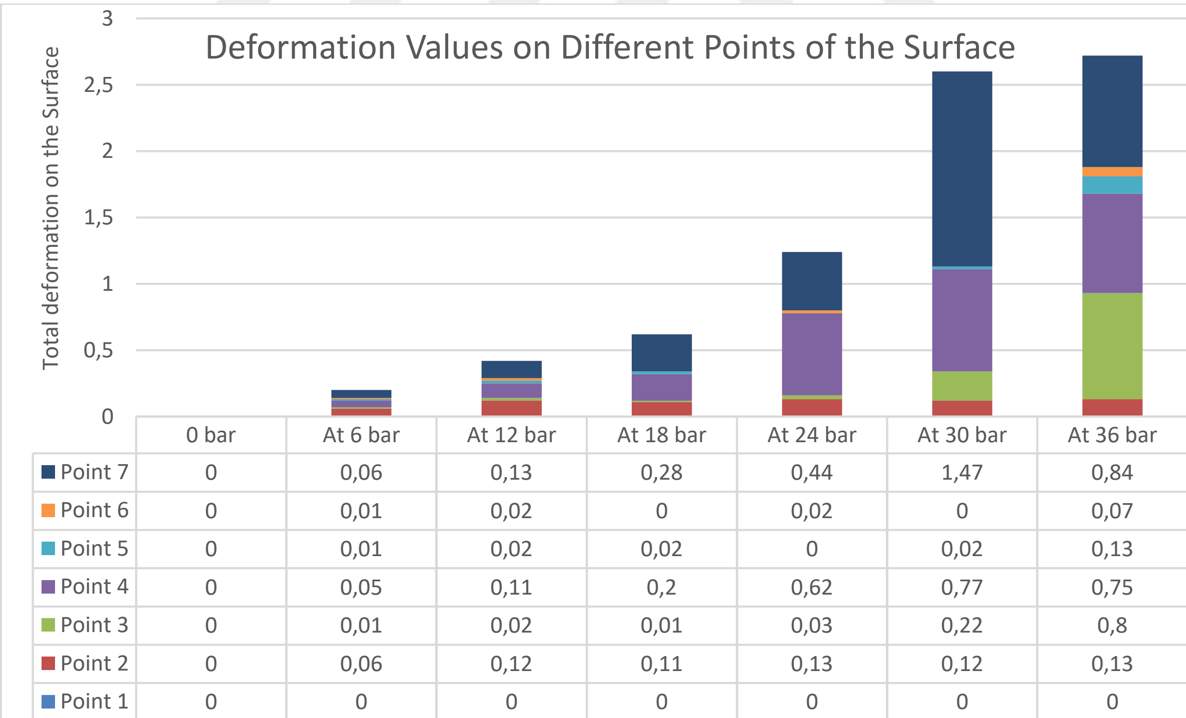

Table 4.29. Total Deformation on the Surface Measurement Points for 0.5 mm AISI 316L Top Plate Used PHE

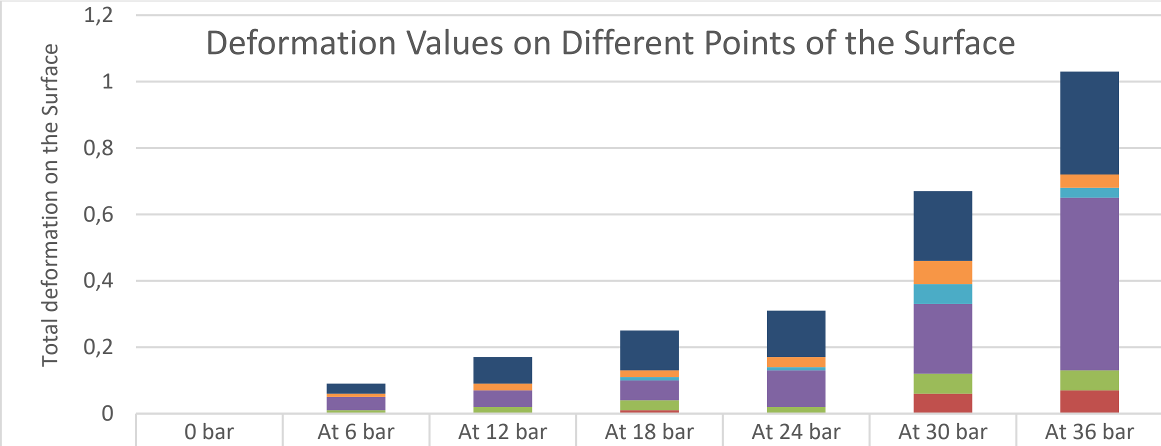

	0 bar	At 6 bar	At 12 bar	At 18 bar	At 24 bar	At 30 bar	At 36 bar
Point 7	0	0,03	0,08	0,12	0,14	0,21	0,31
Point 6	0	0,01	0,02	0,02	0,03	0,07	0,04
Point 5	0	0	0	0,01	0,01	0,06	0,03
Point 4	0	0,04	0,05	0,06	0,11	0,21	0,52
Point 3	0	0,01	0,02	0,03	0,02	0,06	0,06
Point 2	0	0	0	0,01	0	0,06	0,07
Point 1	0	0	0	0	0	0	0

During the testing procedure, the sample was subjected to pressure increments of 6 bar. At each interval, the process was halted, and the sample was extracted. The water present in the sample was then drained and subsequently transferred to the measuring instrument. Measurements were conducted within the domain of meteorology, as explicated by the markers delineated in Figure 40. Subsequently, the specimen was repositioned onto the fixation platform and exposed to compression. Upon reaching a pressure of 12 bar, the component was subjected to an isobaric process for a duration of 180 seconds. Subsequently, the system underwent evacuation, following which deformation measurements were conducted on the heat exchanger and duly recorded. The procedure was consistently executed until reaching a pressure of 36 bar, whereby the corresponding measurements were meticulously recorded and subsequently organized in tabular form. Five different samples have been used and average values are used in the Table 4.27.

Table 4.27 reveals that the entrance and exit points of the channels, which facilitate the direct flow of mains pressure, are situated beneath the surfaces denoted as points 4 and 7 in Figure 4.11. The deformation values acquired at said surfaces surpass the deformation values obtained at other locations. Nevertheless, the distortion at other designated locations is comparatively lower as it is not in immediate contact with the pressurized conduit. The significance of employing this technique lies in its ability to gauge the observable distortion occurring within a given specimen and at what level of pressure.

4.4. Finite Element Analysis Result of AISI 316L 0.5 mm Top Plate Used PHE

The validation of data obtained through experimental methods was completed through FEA analysis, which was based on controlled parameters and enforced findings. The analysis revealed that values close to the results obtained in the experimental method were found and a correlation was established.

Table 4.30. Load Profile Used in Experimental Method

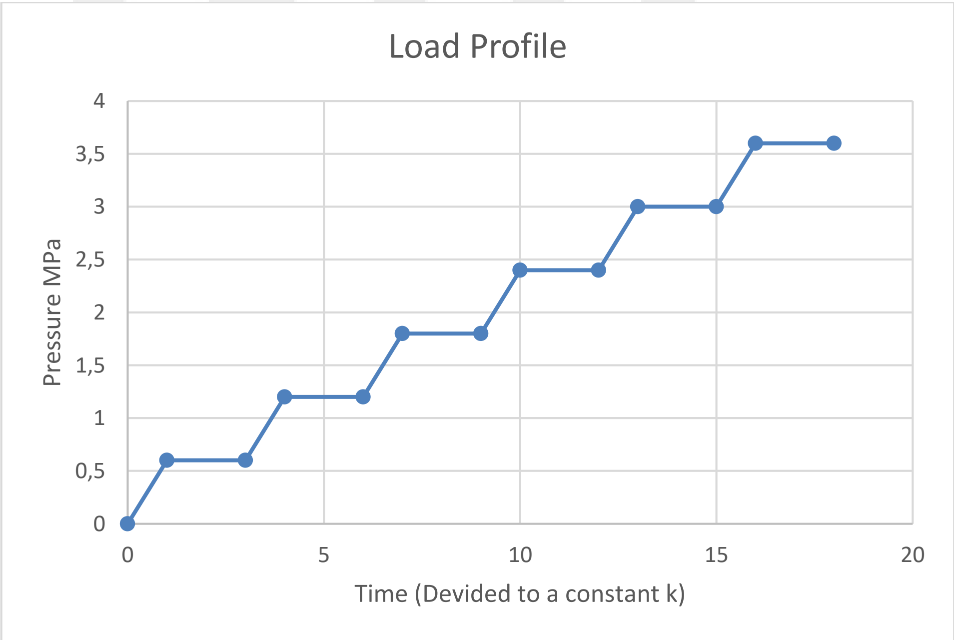

The time-dependent deformation value in finite element analysis is indicated stepwise in the Figure 4.14.

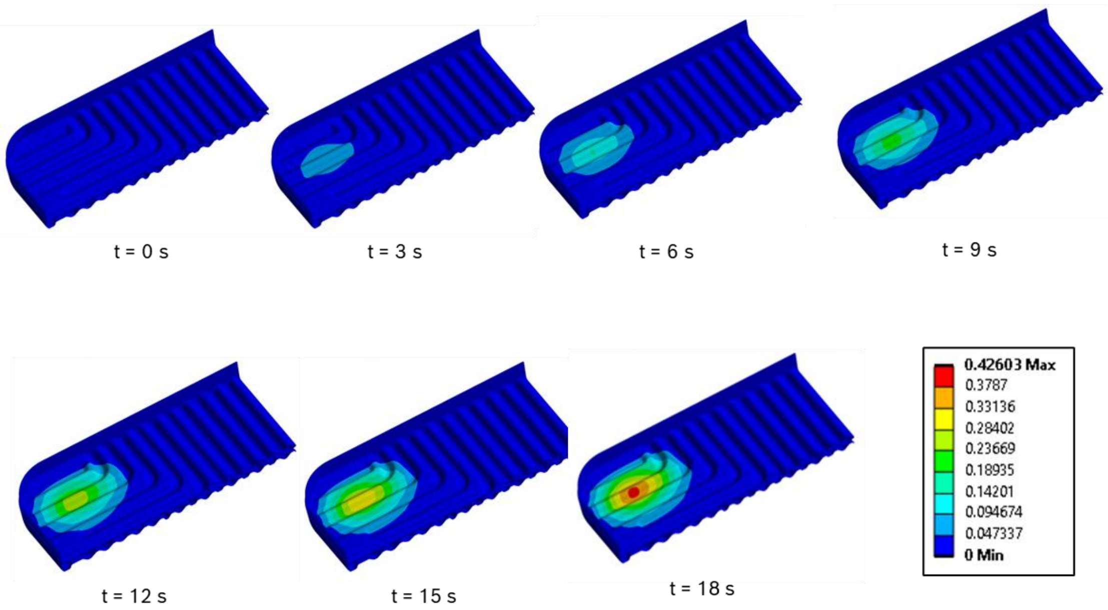

Figure 4.14. Top Plate Deformation with timescale (divided to constant k)

According to Figure 4.14, visual deformation begins to occur between 9*k seconds and 12*k seconds. The values in question correspond to the range of 20 to 25 bar, as indicated in Table 30. Empirical evidence has revealed that this deformation occurs after 24 bar, thereby confirming the correlation between the experimental system and the finite element solution.

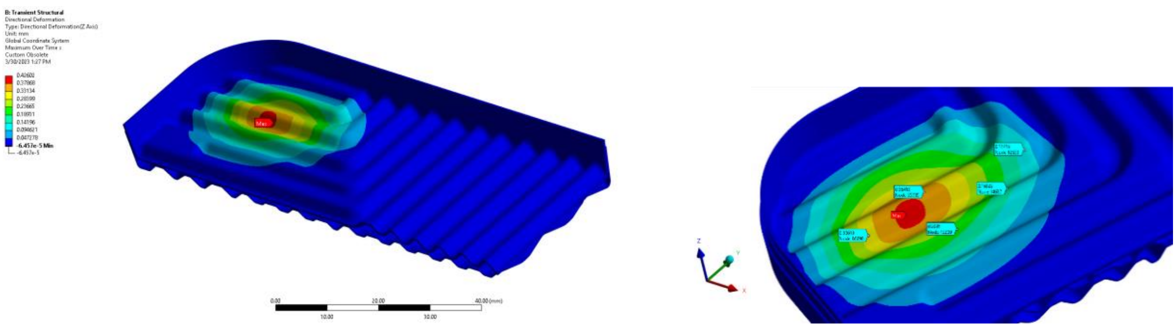

Figure 4.15. Maximum Deformation Calculation Result

The maximum deformation obtained after a gradual pressure increase up to 36 bar is 0.43 millimeters. The measured average value obtained using the probe device is deemed sufficiently close to the relevant correlation for establishment purposes.

The AISI 316L material exhibits a yield stress value of 229.57 MPa. The top plate has been color-coded to indicate regions that exhibit stress values surpassing the threshold limit. These areas are represented by the color red. Figure 4.16 illustrates the potential yield point that may arise on the component after the utilization of 36 bar of domestic pressure.

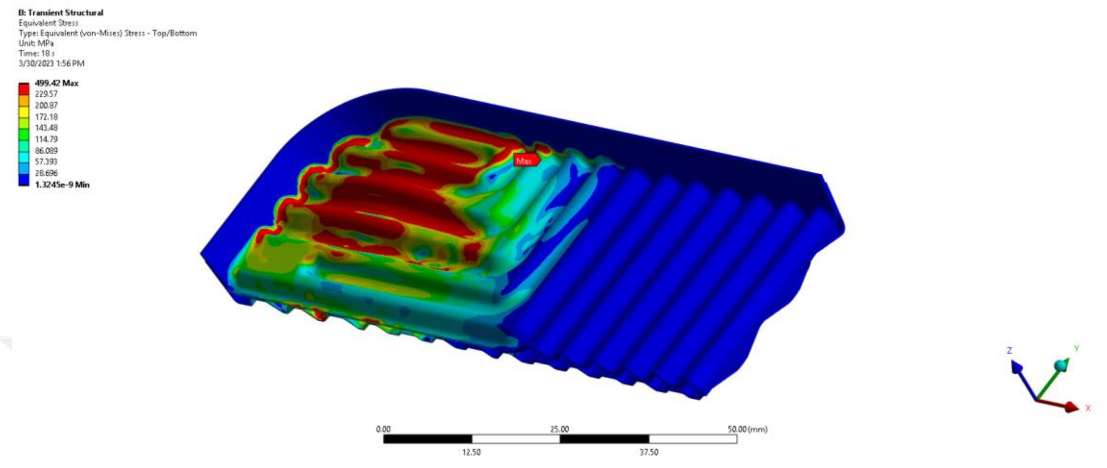

Figure 4.16. Equivalent (Von-Mises) Stress on Top Plate After 36 bar Usage

4.5. AISI 304L 0.5 mm Functional Test Results

There are established standards regarding the output limits of usage conditions during the design phase of each functional element. The component must provide the desired output within the specified range. The standards for plate heat exchangers are regulated in documents such as EN625 and VDS. The thermal performance values are directly related to the internal plate materials and contact surfaces where heat transfer is intensive.

The modification mentioned in this study pertains to the upper plate material, and it is anticipated that the thermal performance impact of this modification will be minimal. However, the thinning of the material does not entail any change in the type of material, thus it does not lead to differences in the thermal performance characteristics.

The functional tests related to plate heat exchangers, featuring a top plate of AISI 316L 0.5 mm, were conducted using a specific quantity of samples comprising 26 plates, and the outcomes were documented. As anticipated, it was noted that there was no discernible variation in thermal performance metrics, thereby eliminating the need to conduct tests using samples featuring varying plate numbers.

The functional tests involved linking the pertinent material to the test configuration, specifying the prescribed temperature levels at designated locations in the reference values, and subsequently ascertaining the temperature flow and pressure values of the fluid at the inlet and outlet points of the plate heat exchanger product. Upon determination of these values, the productivity of the sample was computed using pertinent calculations and subsequently compared against the acceptance criteria. The significance of the analysis results pertaining to the CH line is of utmost importance in this study, given the correlation between the material alteration in the upper plate and the water in the CH line.

Another aspect that warrants assessment is the variation in welding efficacy and thermal conductivity resulting from alterations in the material. The functional test results indicate that there were no issues observed at the welding points of the heat exchanger that contained the 304 and the top plate. Moreover, there was no evidence of heat transmission loss between the materials. The product has successfully passed the functional test, and the obtained results have been documented.

4.5.1. AISI 304L 0.5mm Top Plate Used PHE 26 Plate Functional Test Result

Table 4.31. Functional Test Results for 26 Plates (AISI 304L Top)

Test Results for AISI 304L Top PHE 26 Plates								
		Acceptance Criteria			Test Results		
Description	**Unit**	**Nom**	**Min**	**Max**	**Sample 1**	**Sample 2**	**Sample 3**
CH Flow Rate	l/min	25.1	25	25.2	25.1	25.0	25.1
Temp. CH IN	°C	71.6	70.6	71.6	71.4	71.4	71.5
Temp. CH OUT	°C	51	49.5	52	50.8	50.8	50.8
DHW Flow	l/min	10.1	10	10.2	10.1	10.2	10.1
Temp. DCW	°C	10	9	10	9.7	9.8	9.5
Temp. DHW	°C	60	59.5	61	59.5	59.7	59.6

Table 4.32. Functional Test Results for 26 Plates (AISI 304L Top)

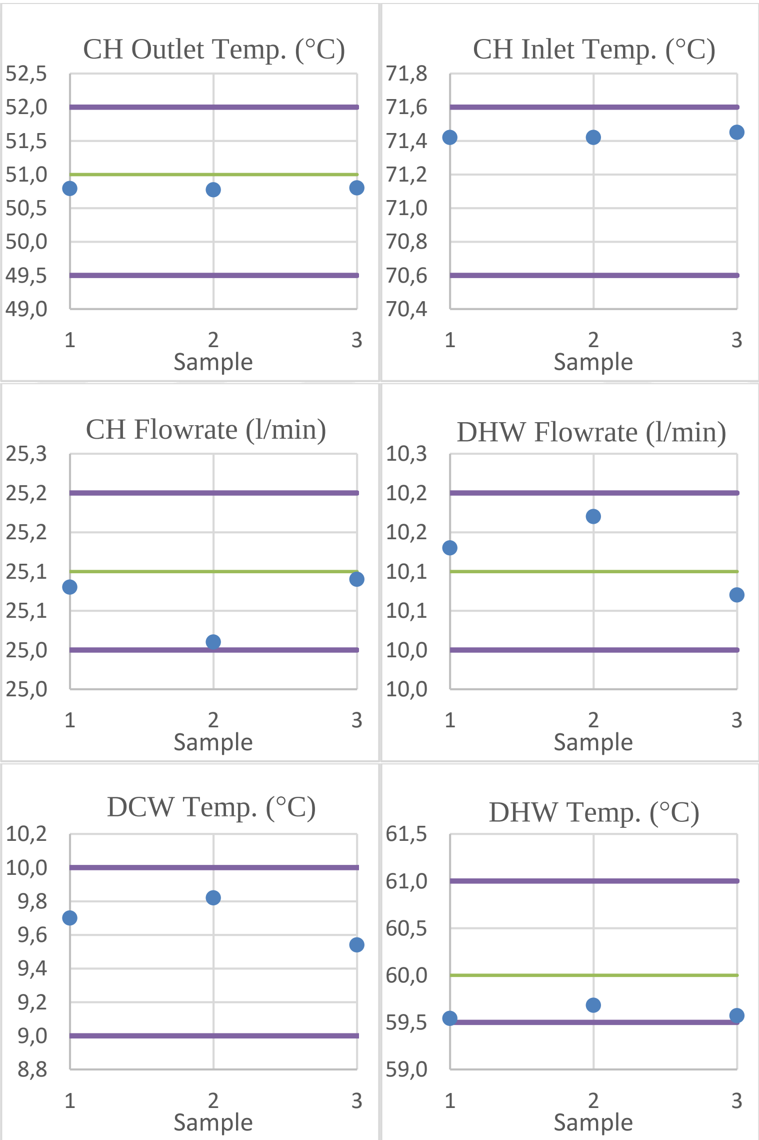

4.5.2. AISI 304L 0.5mm Top Plate Used PHE 24 Plate Functional Test Result

Table 4.33. Functional Test Results for 24 Plates (AISI 304L Top)

Test Results for AISI 304L Top PHE 24 Plates								
		Acceptance Criteria			Test Results			
Description	**Unit**	**Nom**	**Min**	**Max**	**Sample 1**	**Sample 2**	**Sample 3**	
CH Flow Rate	l/min	21.5	21.4	21.6	21.5	21.5	21.5	
Temp. CH IN	°C	72	71	72	71.4	71.4	71.4	
Temp. CH OUT	°C	51	49.5	52	50.8	50.9	50.9	
DHW Flow	l/min	8.5	8.4	8.6	8.6	8.5	8.4	
Temp. DCW	°C	10	9	10	9.6	9.6	9.6	
Temp. DHW	°C	60	59.5	61	60.3	60.2	60.4	

Table 4.34. Functional Test Results for 26 Plates (AISI 304L Top)

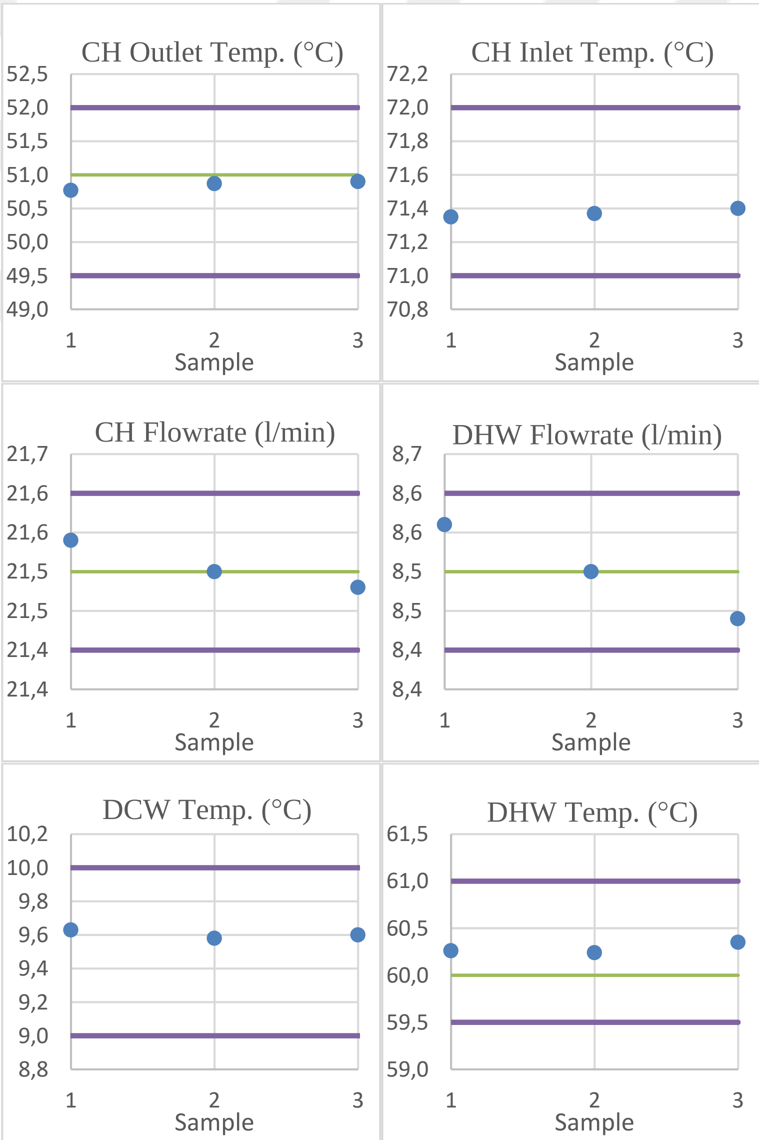

4.5.3. AISI 304L 0.5mm Top Plate Used PHE 24 Plate Functional Test Result

Table 4.35. Functional Test Results for 26 Plates (AISI 304L Top)

Test Results for AISI 304L Top PHE 20 Plates							
		Acceptance Criteria			Test Results		
Description	**Unit**	**Nom**	**Min**	**Max**	**Sample 1**	**Sample 2**	**Sample 3**
CH Flow Rate	l/min	17	16.9	17.1	17.0	17.0	17.0
Temp. CH IN	°C	72	71	72	71.2	71.4	71.5
Temp. CH OUT	°C	51	49.5	52	50.5	50.8	50.6
DHW Flow	l/min	6.9	6.8	7	6.9	6.9	6.9
Temp. DCW	°C	10	9	10	9.8	9.7	9.7
Temp. DHW	°C	60	59.5	61	60.0	60.1	60.1

Table 4.36. Functional Test Results for 26 Plates (AISI 304L Top)

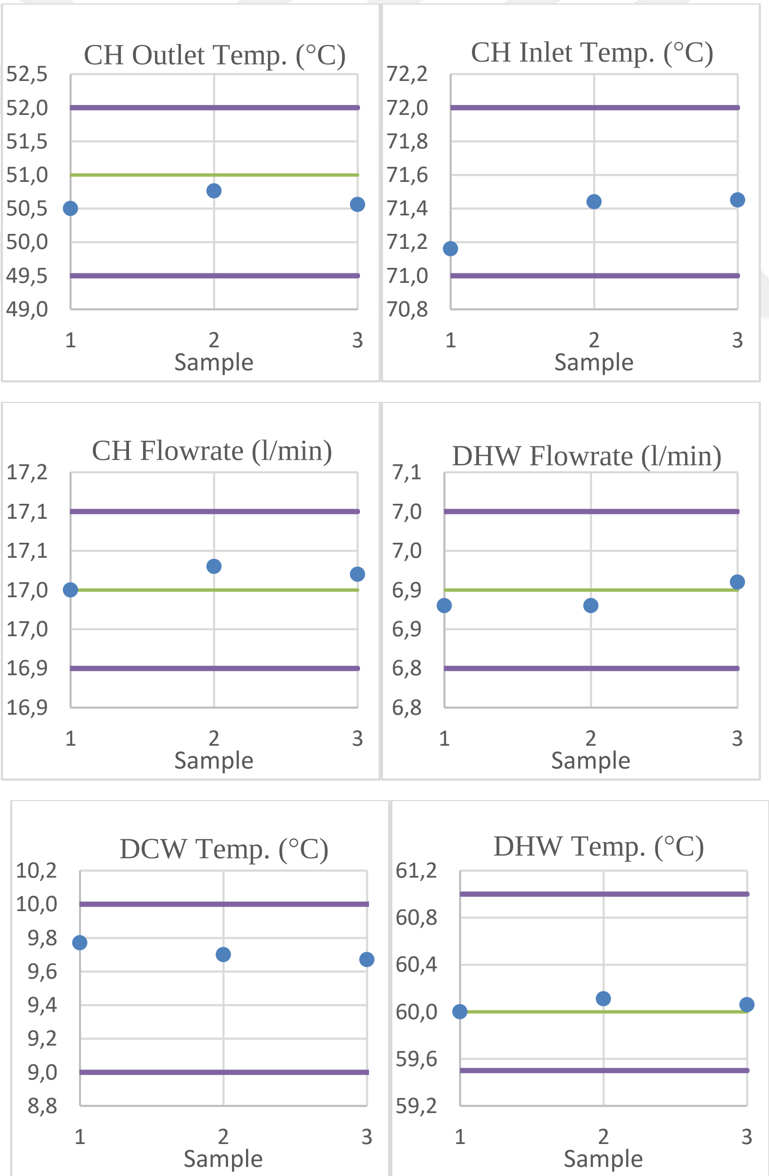

Reduction in thickness of the AISI 304L material, which belongs to a different material family, necessitates the consideration of certain issues due to the varying component ratios it contains. The main topics that can be derived from these points are formability, causality, and corrosion resistance. A decision has been made to subject plate heat exchangers containing AISI 304L 0.5 mm top plate to functional testing to examine and interpret the differences that may arise from the use of new materials. Three separate samples of materials with different plate numbers, namely 26, 24, and 20, were subjected to testing using a functionally specified test apparatus as detailed in the methodology section. It has been demonstrated that the elements have successfully fulfilled their thermal conductivity function, and the output values specified in the relevant standards have been achieved across all samples.

4.6. AISI 316L 0.5 mm Functional Test Results

Table 4.37. Functional Test Results for 26 Plates (AISI 316L Top)

Test Results for AISI 316L Top PHE 26 Plates							
		Acceptance Criteria			Test Results		
Description	**Unit**	**Nom**	**Min**	**Max**	**Sample 1**	**Sample 2**	**Sample 3**
CH Flow Rate	l/min	25.1	25	25.2	25.1	25.1	25.1
Temp. CH IN	°C	71.6	70.6	71.6	71.4	71.2	71.6
Temp. CH OUT	°C	51	49.5	52	51.0	50.4	51.0
DHW Flow	l/min	10.1	10	10.2	10.1	10.2	10.1
Temp. DCW	°C	10	9	10	9.5	9.6	9.5
Temp. DHW	°C	60	59.5	61	59.5	59.6	59.6

4.7. Overall Test Results

Table 4.38. Overall Test Results

Sample No	Deformation After Burst Test (36 bar (10 bar X 3.6 SF))			Functional Test Results Without Any Deformation		
	1 mm AISI 316L Top Plate	0.5 mm AISI 316L Top Plate	0.5 mm AISI 304L Top Plate	1 mm AISI 316L Top Plate	0.5 mm AISI 316L Top Plate	0.5 mm AISI 304L Top Plate
1	No	Yes (24 bar)	Yes (16 bar)	OK	OK	OK
2	No	Yes (24 bar)	Yes (16 bar)	OK	OK	OK
3	No	Yes (24 bar)	-	OK	OK	OK
4	No	Yes (24 bar)	-	OK	OK	OK
5	No	Yes (24 bar)	-	OK	OK	OK
6	No	Yes (24 bar)	-	OK	OK	OK

Upon evaluation of all test results, it has been determined that there is no obstacle to utilizing 0.5 mm AISI 316L material as the upper plate. It has been determined that a deformation of 24 bar can be observed in the component designed and produced with this material. The pressure value exceedingly twice the normal operating pressure value ensures the safe utilization of this material.

The functional tests of exchangers produced using AISI 304L 0.5 mm upper plate material have achieved the desired heat output ranges, but the mechanical strength tests have yielded a lower performance value compared to the alternative material. Notwithstanding this fact, the test has yielded positive results, and the substance has been deemed appropriate for utilization in accordance with the test parameters and transition benchmarks established by the EN625.

5. DISCUSSION

Combi device is a system that provides heating of the central heating line and the domestic water. While the primary heat exchanger provides the heating of the heating line, the heating of the domestic water is provided by the plate heat exchanger located in the combi hydraulic module. The hydraulic unit is a module that provides the flow of water in the device, which includes a plate heat exchanger, pump, and some different functional components, which are generally located at the bottom of the combi boilers. The plate heat exchanger is a component that ensures the realization of heat transfer between the hot heating line water coming from the primary heat exchanger and the cold domestic water coming from the domestic line. This component, which contains steel plates welded to each other by brazing method, has flow lines formed by the welded plates and do not mix with each other. This line works on the cross principle and the heating water passes from one line and the domestic water from the other line. The main factors affecting the actual heat transfer are the width of the channel, the difference in the chevron angle, and the amount of surface area that the water encounters.

Plate heat exchangers contain upper and lower cover plates and inner plates. The plates on which the performance of the heat transfer is evaluated are the inner plates. The outer plates are the elements that provide the mechanical strength of the plate and its protection against external factors. While producing plate heat exchangers, sheet metal of certain thickness and brazing element (copper foil) rolled into rolls are fed into a line at the same time.

These two materials, which encounter each other at the lower and upper points, are shaped with the relevant printing elements.

These shaped plates are grouped, and the upper and lower plates are added to this group. This grouped product is then subjected to a load of 175 kg. After this load, a tight fit occurs between the plates. After the tight fit, a dead weight is placed on the products, and it is aimed to keep this transition constant. Then the products are given to the oven. The main purpose of giving it to the furnace is to melt the copper foil and create brazing points between the metal plates, which can also be interpreted as welding points. After this process, which takes place at a temperature between 1130 and 1150 degrees Celsius, the plate heat exchangers are finalized, and then the product is shipped to the stock area and then to the assembly area after being subjected to leak tests performed with air.

In this thesis, the thickness reduction study on the top plate of the plate heat exchanger used in the industrial field and the application of alternative material with different chemical composition was examined by experimental and numerical methods.

The performance values of these materials were defined, and some inferences were provided regarding their usage in mass production. The parameters affecting the selection of the material used were evaluated, especially the formability, weldability, corrosion resistance, and because of these evaluations, it was decided that the appropriate materials would be AISI 316L and AISI 304L with reduced thickness.

Afterwards, the test methods to be subjected to the selected materials, the possible effects of the change at the component level were determined with the support of the literature research and the appropriate test methods were selected.

Although AISI 316L top plate is the material that also being used in current plate heat exchangers with its 1 mm thickness, AISI 304L is a material that has not been used within the company before. In AISI 316L 0.5 mm transition, the inner plates are not affected, and it is predicted that the brazing points in the lower and upper plate contact will not cause a change in the performance parameters due to the use of the same type of metal material usage.

The burst test, which will measure the mechanical strength performance of the component, was applied, the pressure value at which material began to show plastic deformation was determined and the safety factor of the product was calculated with this output.

This situation is different for the AISI 304L. It has been estimated that the weld strength will be different due to the material change in the lower and upper plates, and it has been concluded that the thermal performance may be affected accordingly. In the light of this information, plate heat exchangers produced with 0.5 mm AISI 304L top plate were subjected to a functional test. The purpose of the functional test is to read the values such as adjustable pressure, temperature, and flow rate in the apparatus from the screen and to calculate the efficiency of the used heat exchanger product with these values. Three different plate numbers, 20-24-26, and three different numbers of samples from each group were used in the tests.

Two of these samples, which passed the functional tests positively, were subjected to burst test to evaluate the mechanical strength performance. Burst test was used to determine the mechanical strength performance of the material. Among these test equipment’s, there is a holder that ensures the fixation of the heat exchanger to test stand and a pump which is used for pressurization in this heat exchanger.

In the study, two different pump types, manual and electronic, were used as pressurization elements. It has been determined that the pressurization time curve of the manual pump is not as linear as in the use of an electronic pump, and the parameters in the experimental setup can be controlled more with the electronic pressurization element.

First, heat exchangers were tested in the manually operated pump, and sudden pressure increases could not be prevented. For this reason, an electronic pressurization tool, which is a more controllable test system element, was used. In this way, gradual pressure increases were realized in the desired time, and this contributed greatly to the transfer of the results to the simulation environment.

As a result of the burst tests, the strength safety factor of the AISI 304L top plate material, which exhibits a lower material strength compared to the AISI 316L material, was calculated as 1.6. This evaluation was made only on two plate heat exchangers and the number of tests could not be increased.

It should be noted that this result may be due to uncontrollable production parameters. As stated in Yiğit Hayta's master's thesis before, the lifetime evaluation test was completed with the heat exchanger using AISI 304L top plate, with the water hammer effect, and success was achieved in these tests. It was determined that the material showed the required mechanical strength at normal usage pressure, but this strength was lower than AISI 316L.

There are two different ways to increase the material strength in the AISI 304L 0.5 mm top plate. These are replacing the purchased raw material with a material containing larger grain size or replacing the used design on the top plate with a pattern that better accommodates the burst effect. In conclusion, AISI 316L 0.5 mm top plate started to deform at 24 bar usage, AISI 304L top plate started to deform at 16 bar usage.

The deformation amounts were obtained with cross sectional cutting of the deformed samples and measuring the channel dimensions on 4 different surfaces for each sample. With the support of ImageJ required values have been measured. However, after these measurements, it was predicted that a spring back effect might occur on the relevant surfaces with a degree of freedom that surface gets after the section cut. It was assumed that this would have an increasing effect on the measured amount. For this reason, the deformation that occurred in AISI 316L was measured with a different method.

A different deformation measurement method was used as a measuring tool with probe. In this method, the sample was not cut and the deformation value on the top plate was measured for each 6 bar pressure increment as delta and noted.

After the deformation data were obtained, the test conditions for the realization of these data were analyzed with the FEA method. As a result of the simulation run, the findings of experimental studies were validated. Quarter model method was used for this simulation study and permanent contacts were assigned to simulate the welding points. A friction coefficient of 0.195 was used at the other points that are predicted to come into contact because of deformation. This value was used in previous simulation studies and since it gave positive results. The applied material values were drawn from the Granta database. These values were calculated in previous studies with the relevant tensile tests and were used with the same references in this study. Mesh assignment was completed after the sensitivity calculations, with mesh quality at 0.88. It is better to have it close to 1 and our value were sufficient for necessary calculation.

Afterwards, the gradual increase in pressure was applied on the determined surface and the deformation in the relevant area was simulated. The results obtained with the experimental method have been validated. This simulation platform that has been constructed with this study has many rooms for improvement and will shed light on many alternative material studies before the investment required for the experimental cost of the materials. With the output, there will be clear information about the adequacy of the burst performance resistance of the material and whether the investment will be beneficial.

6. CONCLUSION AND RECOMMEDENTATIONS

According to the findings of the market research, it has been determined that the utilization of AISI 304L material is common in the context of plate heat exchangers. The examination of a thinning process for the top plate has revealed significant potential for cost savings in annual production figures. Consequently, initiatives were undertaken to reduce the thickness and replace the material of the top plate of the plate heat exchanger. Initially, an assessment was conducted by reaching out to the BOSCH-endorsed APERAM vendor to determine the accessibility of AISI 304L and AISI 316L materials, as well as the feasibility of obtaining the latter in a thickness of 0.5 mm rather than 1 mm. During supplier negotiations, it was communicated that sheets with thicknesses of 0.3 mm, 0.5 mm, and 1 mm are available and deemed appropriate for employment in the pertinent materials. It was determined that the thickness of 0.3 mm utilized in the inner plate would not be suitable for the upper plate. The rationale behind this is rooted in the notion that the upper plate serves as the primary barrier against external impacts. It has been posited that a thickness of 0.3 mm is inadequate to effectively fulfill this protective function. Additionally, the edges of the plate, when fashioned with a 0.3 mm thickness, may experience post-processing shrinkage, colloquially referred to as "undulation". The selection of top plate material was made, opting for 0.5 mm AISI 304L and 0.5 mm AISI 316L as a substitute for the presently utilized AISI 316L 1 mm. Furthermore, assessments designed to evaluate the parameters associated with this alteration were identified. This study conducted mechanical strength and thermal function tests on AISI 304L 0.5 mm top plate material and AISI 316L 0.5 mm top plate material used plate heat exchangers. The obtained results were subjected to thorough analysis.

Functional tests were conducted on plate heat exchangers that were manufactured using AISI 304L and AISI 316L 0.5 mm top plate. The tests yielded positive results and the resultant values were assessed. Subsequently, the products underwent a pressurization test, commonly referred to as a burst test, to assess and analyze their mechanical strength thresholds.

The plate heat exchanger fabricated using AISI 316L 0.5 mm top plate exhibited deformation at a pressure of 24 bar, whereas the plate heat exchanger fabricated using AISI 304L 0.5 mm top plate displayed deformation at a pressure of 18 bar. The determination was made that the quantity of assessments conducted was inadequate for the purpose of utilizing the AISI 304L top plate in mass production.

It was recommended that the quantity of tests be augmented, as the test results were compliant with the EN625 test criteria. However, it is important to note that the operating conditions entail a 10 bar pressure on the mains line, and there exists a possibility that this value may escalate during the initial filling phase.

The inability to generate fresh specimens and expand the quantity of examinations was attributed to the limitations in materials provided by the supplier. A Finite Element Analysis (FEA) technique was devised to simulate the pressurization experiment for the purpose of validating its outcomes. This methodology enables the validation of outcomes in the actual examination, thereby facilitating the preliminary assessment of the pressurization test without incurring material expenses.

Following a series of assessments and supplementary experiments that were not expounded upon in the thesis, plate heat exchangers featuring a top plate thickness of 0.5 mm and constructed from AISI 316L material were incorporated into large-scale manufacturing operations as of June 2023. No errors have been detected within the scope of the modification implemented in this product, which has been in active use in the field for approximately one year. The production process has been ongoing without any deviations from this approach. The simulation platform, which was established utilizing the Finite Element Analysis (FEA) methodology as outlined in the thesis, is presently being utilized for the purpose of conducting research on alternative materials. The implementation of AISI 304L material has been halted because of ongoing assessments of alternative materials. Research efforts aimed at identifying cost-effective materials that can facilitate the production of high-quality products are currently underway.

REFERENCES

Afshari, F., Tuncer, A. D., Sözen, A., Variyenli, H. I., Khanlari, A., & Gürbüz, E. Y. (2021, June 14). A comprehensive survey on utilization of hybrid nanofluid in plate heat exchanger with various number of plates. International Journal of Numerical Methods for Heat & Fluid Flow, 32(1), 241–264. https://doi.org/10.1108/hff-11-2020-0743

Bell, I. H., & Groll, E. A. (2011, April). Air-side particulate fouling of microchannel heat exchangers: Experimental comparison of air-side pressure drop and heat transfer with plate-fin heat exchanger. Applied Thermal Engineering, 31(5), 742–749. https://doi.org/10.1016/j.applthermaleng.2010.10.019

Bento, M. I. F. (2018). Utilização de ferramentas de melhoria contínua na conceção de projeto automóvel (Doctoral dissertation, Instituto Politecnico do Porto (Portugal)).

Büyükaşik, C. (2020) Computational heat and fluid flow analysis of an innovative plate for a plate heat exchanger (Master's thesis, Fen Bilimleri Enstitüsü).

Drienovská, J., & Tvrdá, K. (2017). Deflection of a beam considering the creep. Procedia engineering, 190, 459-463.

Elias, M. M., Saidur, R., Ben-Mansour, R., Hepbasli, A., Rahim, N. A., & Jesbains, K. (2018, April 4). Heat transfer and pressure drop characteristics of a plate heat exchanger using water based Al2O3 nanofluid for 30° and 60° chevron angles - Heat and Mass Transfer. SpringerLink. https://doi.org/10.1007/s00231-018-2335-1

Erdemir, H. (2017). A study on stress corrosion cracking of plate-like heat exchangers and preparation of a test stand to investigate it (Master’s thesis, Fen Bilimleri Enstitüsü)

Erdinç, T. (2019) Yeni bir sıvı-sıvı plakalı ısı değiştiricisinin sayısal ve deneysel olarak incelenmesi (Doctoral dissertation, Osmaniye Korkut Ata Üniversitesi, Fen Bilimleri Enstitüsü)

Fedorov, V., Uhlig, T., Wagner, G., Langohr, A., & Holländer, U. (2019). Influence of nitrogen in brazing atmospheres on the hardness of the microstructural constituents of brazed stainless-steel joints. IOP Conference Series: Materials Science and Engineering, 480(1). https://doi.org/10.1088/1757-899X/480/1/012034

Fukikoshi, T., Watanabe, Y., Miyazawa, Y., & Kanasaki, F. (2014, August 1). Brazing of copper to stainless steel with a low-silver-content brazing filler metal. IOP Conference Series: Materials Science and Engineering, 61, 012016. https://doi.org/10.1088/1757-899x/61/1/012016

Gatea, S., Ou, H., & McCartney, G. (2016, February 23). Review on the influence of process parameters in incremental sheet forming. The International Journal of Advanced Manufacturing Technology, 87(1–4), 479–499. https://doi.org/10.1007/s00170-016-8426-6

Gullapalli, V. S., & Sundén, B. (2013, September 30). CFD Simulation of Heat Transfer and Pressure Drop in Compact Brazed Plate Heat Exchangers. Heat Transfer Engineering, 35(4), 358–366. https://doi.org/10.1080/01457632.2013.828557

Gürler, Y. (2018a). Design and mechanical behaviour of brazed plate heat exchangers (Doctoral dissertation, Izmir Institute of Technology (Turkey)).

Gürler, Y. (2018b). Design and mechanical behaviour of brazed plate heat exchangers (Doctoral dissertation, Izmir Institute of Technology (Turkey)).

Hacısalihoğlu, M. (2021). Su esası CuO nanoakışkan için plakalı ısı değiştirgecinde performans incelemesi. (Doctoral dissertation, Karadeniz Teknik Üniversitesi, Fen Bilimleri Enstitüsü)

Hana, Y. (2015). A Characterization of Flat-Plate Heat Exchangers for Thermal Load Management of Thermoelectric Generators (Doctoral dissertation).

Hayhurst, D. R. (1972). Creep rupture under multi-axial states of stress. Journal of the Mechanics and Physics of Solids, 20(6), 381-382.

Hayta, Y. (2020). Investigation of the Fatigue Behaviour of Metallic Components Used in Plate Heat Exchangers Under Variable Dynamic Loads (Master's Thesis, Izmir Institute of Technology (Turkey)).

Hussaini, S. M., Singh, S. K., & Gupta, A. K. (2014, January). Experimental and numerical investigation of formability for austenitic stainless steel 316 at elevated temperatures. Journal of Materials Research and Technology, 3(1), 17–24.https://doi.org/10.1016/j.jmrt.2013.10.010

Inamdar, H. V., Groll, E. A., Weibel, J. A., & Garimella, S. V. (2023, February). Air-side Fouling of Finned Heat Exchangers: Part 1, Review and Proposed Test Protocol. International Journal of Refrigeration. https://doi.org/10.1016/j.ijrefrig.2023.02.017

Jayahari, L., Sasidhar, P., Reddy, P. P., BaluNaik, B., Gupta, A., & Singh, S. K. (2014, January). Formability studies of ASS 304 and evaluation of friction for Al in deep drawing setup at elevated temperatures using LS-DYNA. Journal of King Saud University - Engineering Sciences, 26(1), 21–31. https://doi.org/10.1016/j.jksues.2012.12.006

Kocabaş, C. (2014). Farklı malzemelerden imal edilmiş plakalı ısı değiştiricilerinin atık ısı geri kazanım performanslarının deneysel analizi (Master's thesis, Fen Bilimleri Enstitüsü).

Kumar, S., Hussein, H. M., & Hussein, A. (Eds.). (2017). AI applications in sheet metal forming. Springer Singapore.

Lijun Yang, Hui Tan, Xiaoze Du, Yongping Yang, (2012) Thermal-flow characteristics of the new wave-finned flat tube bundles in air-cooled condensers, International Journal of Thermal Sciences, Volume 53, https://doi.org/10.1016/j.ijthermalsci.2011.11.002.

Malakoutikhah, H., Madenci, E., & Latt, L. D. (2022, June 2). A computational model of force within the ligaments and tendons in progressive collapsing foot deformity. Journal of Orthopaedic Research, 41(2), 396–406. https://doi.org/10.1002/jor.25380

Onal, O., Bal, B., Canadinc, D., & Akdari, E. (2015, August 6). Experimental and Numerical Evaluation of Thickness Reduction in Steel Plate Heat Exchangers. Journal of Engineering Materials and Technology, 137(4). https://doi.org/10.1115/1.4031080

Peker, G., Yıldız, C., Çakmak, G., Bilgiç, Y., & Yıldız, A. (2022, May 25). Thermal performance of new type plate heat exchanger with spring turbulence generator using nanofluid flow. Experimental Heat Transfer, 1–15. https://doi.org/10.1080/08916152.2022.2081886

Persson, B. (2011). Numerical analysis of a BPHE channel plate section. Division of Solid Mechanics, Lund University.

Ribatski, G., & Thome, J. R. (2007, May). Experimental study on the onset of local dryout in an evaporating falling film on horizontal plain tubes. Experimental Thermal and Fluid Science, 31(6), 483–493. https://doi.org/10.1016/j.expthermflusci.2006.05.010

Şahin M. (2021) Plakalı ısı değiştiricilerinin hesaplamalı akışkanlar dinamiği yöntemiyle performans değerlerinin incelenerek optimizasyonu ve yüksek verimli plaka tasarımı (Master'x Thesis, Fen Bilimleri Enstitsüs)

Sevim, M. (2016). Searching effect of different design parameters on thermal effectiveness of the heat exchanger with numerical methods (Master's thesis, Fen Bilimleri Enstitüsü)

Shah, R. K., & Sekulic, D. P. (2003). Fundamentals of heat exchanger design. John Wiley & Sons

Sigvant, M., Pilthammar, J., Hol, J., Wiebenga, J. H., Chezan, T., Carleer, B., & van den Boogaard, T. (2019). Friction in sheet metal forming: Influence of surface roughness and strain rate on sheet metal forming simulation results. Procedia Manufacturing, 29, 512–519. https://doi.org/10.1016/j.promfg.2019.02.169

Vahab Hassani, James Dickens & Kennett J. Bell (2005) The Fin-on-Plate Heat Exchanger: A New Configuration for Air-Cooled Power Plants, Heat Transfer Engineering, 26:6, 7-15, Doi: 10.1080/01457630590950826

Wolert, P. J. (2019). Reliability-Based Calibration of the Code for Steel Girder Bridges (Doctoral dissertation, Auburn University).

Xu, S., Wang, C., & Wang, W. (2015, May). Failure analysis of stress corrosion cracking in heat exchanger tubes during start-up operation. Engineering Failure Analysis, 51, 1–8. https://doi.org/10.1016/j.engfailanal.2015.02.005

REPUBLIC OF TÜRKİYE
AYDIN ADNAN MENDERES UNIVERSITY
GRADUATE SCHOOL OF NATURAL AND APPLIED SCIENCES

SCIENTIFIC ETHICAL STATEMENT

I hereby declare that I composed all the information in my master's thesis entitled "EFFECT OF MATERIAL CHANGE AT PLATE HEAT EXCHANGER DESIGN TO SYSTEM PERFORMANCE" within the framework of ethical behavior and academic rules, and that due references were provided and for all kinds of statements and information that do not belong to me in this study in accordance with the guide for writing the thesis. I declare that I accept all kinds of legal consequences when the opposite of what I have stated is revealed.

Kadir CEBECİ

18 / 07 / 2023

CURRICULUM VITAE

Last name, First name: Cebeci Kadir

Nationality: Republic of Turkey

Foreign language: English

Education: Bachelor

Level	Institute	Date of graduation
Bachelor’s	Gaziantep University	27/06/2020

WORK EXPERIENCE

Year	Place/Institute	Title
2019-2020	SIEMENS AG	R&D Engineering Intern
2020-2021	YILDIRIM ELSAN (SIEMENS TECHNOLOGY PARTNER)	R&D Project Engineer
2021-2023	BOSCH HOME COMFORT GROUP	R&D Design Engineer